1969

Detection of sodium boiling in fast sodium-cooled reactors by neutron measurements

Keith Eugene Asmussen
Iowa State University

DETECTION OF SODIUM BOILING IN FAST SODIUM-COOLED REACTORS BY NEUTRON MEASUREMENTS

by

Keith Eugene Asmussen

A Dissertation Submitted to the
Graduate Faculty in Partial Fulfillment of
The Requirements for the Degree of
DOCTOR OF PHILOSOPHY

Major Subject: Nuclear Engineering

Approved:

Signature was redacted for privacy.

In Charge of Major Work

Signature was redacted for privacy.

Head of Major Department

Signature was redacted for privacy.

Dean of Graduate College

Iowa State University
Ames, Iowa

1969

TABLE OF CONTENTS

I. INTRODUCTION

To utilize fully the world's energy resources, fast breeder reactors employing uranium and plutonium fuels are necessary (1). The present generation of light water reactors utilize only about 1% of each kilogram of uranium extracted from the earth's crust. The residual 99% remains as an untapped potential source of energy. The neutron economy of a fast reactor permits all uranium, other than processing losses to be converted to energy (2). Furthermore, excess fissionable material produced in a fast reactor may be used as fuel for thermal reactors.

A high volumetric heat removal rate is required for fast reactors to increase the specific power of the costly fuel. This increases the power density and decreases the reactor's dimensions and cost.

Helium (3), steam (4), and liquid sodium are all being actively considered as fast reactor coolants by various organizations. Sodium exhibits excellent heat transfer properties and low operating pressures. These advantages plus more than 20 years of experience (5) with liquid metal heat transfer systems have made liquid sodium the choice in most fast breeder projects.

The stability and safety of fast sodium-cooled breeder reactors depends on a number of reactivity or feedback effects. Five power or temperature coefficients of reactivity

are:

1. Axial fuel expansion coefficient (usually negative),
2. Fuel element bowing due to thermal gradients in fuel elements (may be positive or negative),
3. Radial core expansion coefficient (usually negative),
4. Doppler coefficient, (usually negative),
5. Sodium void coefficient (may be positive or negative).

The reactor's temperature coefficient is equal to the sum of the temperature coefficients of all the various mechanisms which influence reactivity.

The behavior of a reactor following a change in power depends on the sign of the total power or temperature coefficient. For instance, consider an increase in reactor power and hence coolant temperature. If the temperature coefficient of reactivity is positive, the reactivity increases, and as a result, so does the power. This in turn increases the reactivity once more which leads to a further power increase. It is evident that under these circumstances the power will continue to increase until some external intervention brings the reactor under control, or until the core melts. Obviously, a reactor having a positive power coefficient is inherently unstable with respect to power changes.

The sodium void effect is receiving much attention because of the possibility that in some reactors it may yield a potentially dangerous positive coefficient of reactivity. Many papers dealing with the sodium void coefficient have been written (6, 7, 8, 9).

The problem of positive sodium-void effects in large plutonium fueled fast reactors arises from the fact that the fission cross section of Pu-239 decreases less rapidly with increasing energy than do the absorption cross sections of materials in the reactor (6). Also, the number of neutrons produced per fission, $\nu(E)$, increases with energy over the range of interest. This is reflected in the fact that the number of neutrons emitted per neutron absorbed in all materials, η', increases with energy. The inelastic and elastic scattering provided by sodium tends to transfer neutrons from an energy region where η' is high to a lower energy region with a correspondingly lower η'. The result is that the presence of sodium in the reactor reduces the reactivity. Thus when the sodium density decreases due to an increase in temperature, or when accidental sodium boiling occurs, there is spectral hardening and a positive reactivity effect. This spectral hardening can also add reactivity by increasing the number of fertile fissions.

A second sodium-void effect is an increase in neutron leakage from the reactor core accompanying a decrease in

sodium density. This effect reduces the reactivity. However, the magnitude of this effect diminishes with increasing core size. The spectral hardening effect dominates in large reactors.

The sodium-void coefficient is a function of position in the reactor. The leakage component, which is negative, has it's largest magnitude at the edge of the core, and is zero at the center. A void at the center of the core has little effect in a large reactor since the surrounding core material behaves as a reflector. On the other hand, spectral hardening will tend to be most important near the center of the core.

The safety considerations of fast reactors differ from those of thermal reactors mainly because of the much shorter mean lifetime of prompt neutrons (10^{-8}-10^{-6} sec). For small reactivity additions, fast reactor dynamics behave similar to a thermal reactor in being governed by the properties of the delayed neutrons. However, as the excess reactivity approaches the value of the effective delayed neutron fraction the behavior of a fast reactor is characterized by very rapid power increases.

The power level in a reactor behaves approximately as

$$P(t) \simeq P(o)e^{t/T} \qquad (1)$$

after the initial transients have diminished. Here P(t) is the power at some time t following a change in reactivity

at time t=o, and T is the "stable period" of the reactor.

For a step change in reactivity the stable period is approximately (10)

$$T \simeq \frac{\ell_{ave}}{k_{eff}-1}$$

$$\simeq \frac{\ell_{ave}}{\rho} \quad , \tag{2}$$

where ℓ_{ave} is the average time between generations of neutrons and ρ is the reactivity defined as

$$\rho \equiv \frac{k_{eff}-1}{k_{eff}} \quad , \tag{3}$$

where k_{eff} is the effective multiplication factor. As ρ approaches the value of the effective delayed neutron fraction, β_{eff}, the average time between generations approaches the effective lifetime of a prompt neutron in the reactor, ℓ_p. When the reactivity equals the delayed neutron fraction, the reactor is critical on prompt neutrons alone and is said to be "prompt critical".

For a thermal reactor, ℓ_{ave} is of the order 0.1 second and ℓ_p is approximately 10^{-4} second. The effective delayed neutron fraction is around 0.0065. This means that when $k_{eff} \simeq 0.0065$ the reactor is prompt critical and will experience a potentially destructive power excursion described by

$$P(t) \simeq P(0)e^{610t} \quad . \tag{4}$$

In one second the power will increase by a factor of e^{610}.

For a plutonium-uranium fueled fast reactor $\beta_{eff} \simeq 0.0035$ and $\ell_p \simeq 5 \times 10^{-7}$ (11). Due to the smaller value of β_{eff}, k_{eff} needs only to reach $\simeq 1.0035$ to produce a prompt critical reactor. Thus smaller additions of reactivity will cause the reactor to go prompt critical. Furthermore, a much more severe power excursion will result because of the small value of ℓ_p. At prompt critical

$$P(t) \simeq P(0)e^{3.5x10^4 t} \quad . \tag{5}$$

In some cases, the magnitude of the positive sodium-void effect is large enough to override the negative contributions provided by the Doppler effect and other mechanisms which reduce reactivity. It may be possible for the reactor to become prompt critical by losing coolant from part of the core (12). As a result, the positive void coefficient in conjunction with boiling may lead to the destruction of the core.

It is apparent that for the safe and reliable operation of a fast reactor all mechanisms which may add reactivity must be known and monitored. Since local sodium boiling will lead to voiding a portion of the core, it is imperative to prevent boiling or, if boiling occurs, to be aware of the occurrence and take corrective actions. If incipient boiling can be detected soon enough, the reactor may be immediately shut down, preventing destruction of the core. Thus one can

see the importance of sodium boiling and of it's early detection in a fast reactor core.

A sodium cooled fast breeder reactor is designed such that under normal rated operating conditions the coolant will remain well below it's boiling temperature. Only abnormal or accidental circumstances will instigate coolant boiling. Semeria (13) points out that there is a possibility of boiling in a hydraulically intact core if one is dealing with a slow transient. Examples of such slow transients are:

1. An accidental blockage of flow at the base or in the interior of an assembly;
2. A slow-down in pumping capacity;
3. An accidental reactivity addition below a certain rate.

The importance of diagnosing incipient failures such as the above has been the subject of many papers (14).

This study concerns the detection of boiling as a result of such a slow transient. It is the incipient boiling preceding any rapid and destructive power excursion that is of interest here. There are a number of techniques which have been and are currently being studied for the purpose of detecting boiling. These will be reviewed and a technique based on neutron flux noise measurements will be introduced. The space dependent noise formulation to be presented allows cross correlation between neutron energy groups. The theory

of the noise formulation will be applied to a mathematical model of a fast reactor. Boiling in an assembly will be analytically simulated and the spectral and cross spectral density functions for various trial conditions will be presented. Finally, the effect of temperature feedback on the results will be indicated by employing a simple feedback model for various values of the Doppler coefficient.

II. SODIUM BOILING CHARACTERISTICS

Because of its importance in fast reactor dynamics and safety analysis (15, 16), sodium boiling has been the subject of many investigations. Among the boiling phenomena studied are: boiling heat transfer characteristics (17), two-phase flow (18), transient voiding rates (19), pressure pulses (20), void fraction and liquid superheat (17, 21).

Lurie and Noyes (22) made the first significant attempt at development of a digital computer code for the transient analysis of single-channel sodium boiling. MacFarlane (23, 24, 25) eliminated some of the limiting simplifications of this early work. He developed an analytical model to use in performing calculations aimed at predicting the time-dependent behavior of transient boiling sodium coolant in a reactor.

Experimental evidence indicates that large superheats are possible in liquid sodium. This could lead to a highly unstable situation. Highly superheated sodium might suddenly vaporize, thus voiding a large portion of the core. The rate at which a channel is voided depends mainly on the amount of superheat. Clearly it is essential that the amount of liquid sodium superheat be reduced or accurately predicted.

Although it is generally accepted that superheating occurs, there is no such agreement on the actual value of superheat for a given physical system. One laboratory reports superheats up to 224^{o}F for flowing sodium, while a second

laboratory reports superheats of no more than about 25°F have been measured in flowing sodium (21).

The superheat needed to initiate boiling depends on many parameters including system pressure, dissolved gas, texture of heating surface, impurity concentration, heat flux, radiation environment, and the pressure-temperature history (20). This dependence is not fully understood, as evidenced above, and so it is not yet possible to predict the superheat reliably.

Perhaps the safest way to diminish the uncertainties and associated dangers of large superheats is to reduce their magnitude through engineering design of the reactor coolant system. Reducing the superheat, as a means of enhancing the use of alkali metals as coolants, has been suggested by Edwards and Hoffman (26) and by Holtz and Singer (21).

Practically all experiments performed so far have been under conditions significantly different from those to be experienced in a large power reactor. The operating conditions of a large power reactor may themselves tend to reduce the superheat required for boiling.

Experiments with sodium in the United Soviet Socialist Republic have shown that large reductions in liquid superheat are obtained by increasing the pressure and heat flux to fast breeder reactor conditions (27). Atomics International has shown that the maximum measured bulk superheats exhibit a

strong decreasing effect in maximum superheats as pressure is increased (28). It was also observed that little or no superheating is obtained when the sodium velocity is above approximately 4 feet per second (29). Further experiments at Atomics International have indicated that little or no superheating is obtained when the heater surface has been attacked by the sodium, producing well-defined surface prominence and pits (30). Experiments by Heineman (31) at Argonne National Laboratory yielded, superheats which were rather low in comparison to values reported by other experimentors. Furthermore, Heineman's results indicated that the superheat required to initiate boiling decreased with time.

Edwards and Hoffman (26) suggests two methods for reducing the superheat of liquid sodium coolant. First, by increasing the operating temperature and second, by modifying the heating surface, for example by sintering stainless steel particles on the inside tube surface.

Judd (32) discusses a number of conditions which tend to reduce the amount of superheat required to initiate boiling in an operating reactor. One of these is the effect of ionizing radiation.

Energy provided by ionizing radiation may allow bubble nuclei to be formed in the bulk of the liquid as well as in cavities in the heating surface. These additional nucleation sites then lowered the superheat required to produce boiling.

It appears that only "knocked-on" sodium atoms from elastic collisions with fast neutrons and possibly fission fragments are likely to cause nucleation (33). It can be shown that knocked-on sodium atoms produce numerous nuclei which will grow at superheats above 200°C, but a negligible number large enough to grow at lower superheats. Fission fragments have a bigger effect, but this depends on the degree of contamination of the coolant by fissile material. Thus in an operating reactor, the superheat will be limited by radiation effects to about 200°C.

However, Judd also points out that in an engineering system, mechanical considerations may become more important. For example, in a reactor, overheating of the coolant may be accompanied by cracking of the fuel element cladding. This would release bubbles of fission-product gas which could then prevent significant superheating. In addition, in any circulating system entrainment of gas bubbles at the cover gas interface might prevent superheating. One bubble of radius 10^{-3} cm in every cm^3 of liquid sodium would be enough to do this. This corresponds to an average concentration of only 3×10^{-6} parts per million by atoms.

Operation of the sodium-cooled systems SIR, ERB-II, SRE, Fermi and Hallum has provided useful experience. This experience has shown that methods for impurity monitoring and removal in these systems were inadequate, and most have

experienced serious operating difficulties due to the presence of undetected forms of impurities in the primary sodium (5). From this it appears that there may be sufficient concentrations of impurities in an operating reactor to reduce the superheat.

Sodium boiling experiments have also pointed out that as the heat flux is increased the boiling becomes quite stable; once the sodium nucleates, boiling continues indefinitely (21). Similarly it has been observed that boiling becomes more stable as the system pressure is increased.

Thus it is seen that in an operating fast breeder reactor the superheat required to initiate boiling may not be nearly as large as originally anticipated. Conditions may be more nearly those capable of sustaining steady boiling of the coolant during a slow transient. It is just this kind of boiling that one would like to be able to detect so as to protect the reactor system.

Boyd (34) studied the bubble-formation rate in water as a function of heat flux. A stroboscopic light was used to determine the frequency range of bubble formation. In general, the rate was 25-60 bubbles per second over the range of heat fluxes applied. This held true for observations at various different nucleation sites as well as for the same nucleation site for the heat fluxes studied. Thus a signal such as neutron flux perturbations excited by boiling would

be expected to be in this frequency range. Although this work was for water, the behavior of liquid sodium and water are often very similar (35, 22).

Lurie and Noyes (22) found that, as for other liquids (36), the frequency of bubble generation does not vary with the heat flux, but the number of nucleation sites increases. This causes an increase in the amplitude of the signal excited by the boiling perturbation. A spectrum analysis of surface temperature fluctuations under several pool-boiling conditions was also performed by Lurie and Noyes. The relative power spectral density as a function of frequency is shown in Figure 1. The results of the analysis exhibit a distinct resonance frequency of approximately 2 cycles per second. This indicates periodic bubble generation at a nucleation site near the imbedded thermocouple.

Logan et al. (18) report that power spectral density measurements of tape recorded flow signals from boiling sodium experiments indicate the largest components of boiling noise were in the band from 1 to 10 cycles per second. Rajagopal (37) also attributes resonance peaks found in power spectral density measurements, at the Enrico Fermi plant, to nucleate boiling. These peaks occurred between 10 and 15 cycles per second.

As one would expect, sodium boiling appears to be a

low frequency phenomenon. Thus the neutron flux perturbation induced by sodium boiling will be characterized by low frequency noise.

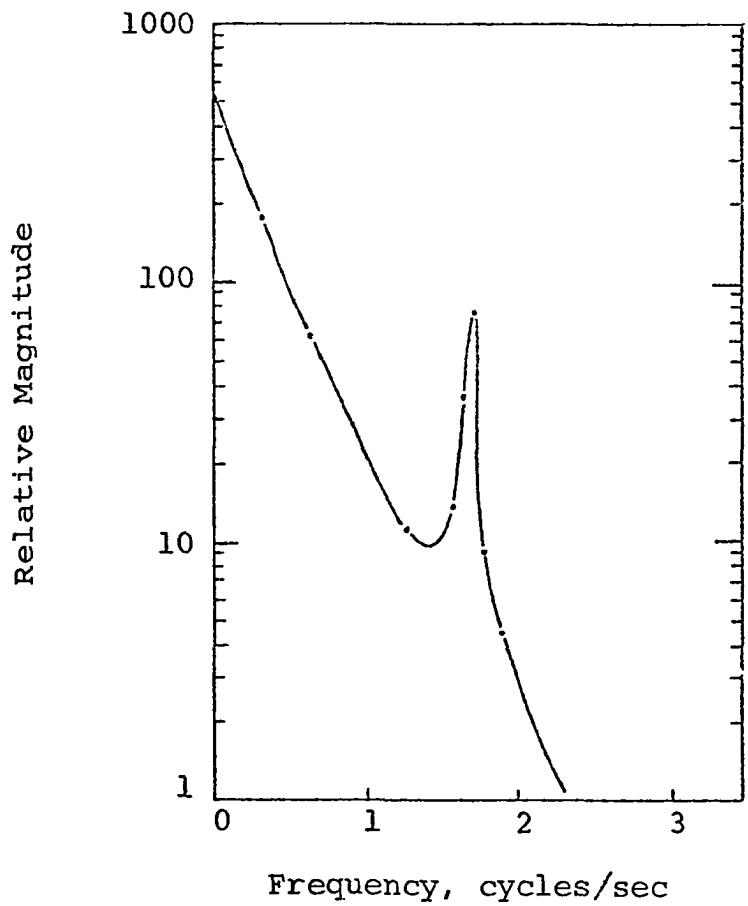

Figure 1. Power spectral density of boiling sodium

III. METHODS OF BOILING DETECTION

A. General Review

Early work related to boiling detection was done at Argonne National Laboratory (38). This work was not concerned with the actual detection of boiling but with measuring the density of a steam-water mixture boiling at 600 psia. Density measurements were based on the attenuation of gamma rays from a thulium source. The purpose was to provide basic information for the Boiling Reactor Experiment. Hooker and Popper (39) continued work in this area concerning themselves with measuring the void fraction in a simulated reactor flow channel. In their work they pointed out the need for a refinement in the technique. At about the same time, O'Brian (40) reported successful measurements in water of void areas of 1%, 3%, and 5% by γ-ray attenuation.

Gouse (41) reviewed the methods of measuring void fractions for the period from 1951 to 1960. The methods then in use were:

1. visual observation
2. γ-ray attenuation
3. x-ray attenuation
4. beta-particle absorption
5. radioactive tracer.

In the visual observation method, photographs were taken

and the bubbles were counted and measured. This suffered from the obvious difficulty of analyzing a three-dimensional problem with two-dimensional data. It was quite a tedious task and required a transparent test section with its obvious limiting conditions.

Three conditions were necessary in applying the radioactive tracer method. First, the radioactive tracer must not appear in the vapor phase or on the tube walls. Second, the counting tube must be exposed to the same volume of pipe at two geometrically similar locations (for calibration). Third, the intensity of radiant energy received by a suitable detector must be proportional to the total amount of tracer in the scanned section, and be essentially independent of flow patterns.

For successful use of the γ-ray or x-ray attenuation method a mono-energetic source is required. The beam of radiation and the detector must be well defined, and the beam intensity must be high enough that statistically good data can be obtained. The beta-particle absorption technique is similar to the x- or γ-ray methods. However the beta-particle technique is complicated by the fact that beta-particles are given off with a continuous energy spectrum and can lose a large fraction of their energy in a single collision.

Gouse found that the then most commonly used method was γ-ray attenuation and the least used method was that using a

radioactive tracer.

Wentz et al. (42) presents a rather complete discussion on x-ray measurement of void dynamics in boiling liquid metals. The theoretical basis, measurement accuracy and space and time resolution of the method is presented. Such measurements can be used to follow the rapid changes of void fraction which occur with boiling in liquid metals.

Balzhiser and Smith (43) and Ferrell and McGee (44) describe in detail instrumentation based on the gamma attenuation technique for measuring two phase metallic flow and void fractions respectively.

The experience gained from this early work in void fraction measurement was later applied to the problem of detecting boiling in water reactor systems. A more recent work by Rouhani (45) describes the use of a turbine type flowmeter in the measurement of steam quality and void.

Obviously the visual method is not applicable to inpile measurements. The high temperatures and radiation environment in a reactor also make it very difficult, if not impossible to fulfill the conditions necessary for the successful employment of the other methods discussed above. The gamma-ray attenuation signal and the radioactive tracer radiation would be indistinguishable in the presence of the high radiation environment present in reactor.

As a result, new techniques had to be found for detecting

boiling in nuclear reactors.

These new techniques had to be first investigated by out-of-pile experiments. Thus the previous experience and methods provided the means by which new techniques could be evaluated. The results of a new method could be compared with those of a known and standardized procedure.

Work on one of the first procedures for detecting boiling in a reactor was done by Katz et al. (46). The detection method was based on the Jens and Lottes equation (47). The Jens and Lottes equation is a relationship between the heat flux, pressure, wall temperature, and saturation temperature of water at conditions of the test. The presence of boiling was established with certainty by means of a pressure-cycle, temperature-cycle technique. By sinusoidally varying the system pressure and observing temperature fluctuations, conclusions could be drawn regarding the presence of boiling in the reactor.

This method might not be practical for application to a power reactor where the systems pressure must remain essentially constant.

Hogan and Boyd (48) endeavored to detect nucleate boiling by listening with hydrophones. Two arrangements were tried. These were, 1) a hydrophone mounted inside the water channel downstream from the boiling area for passive listening to identify any sounds characteristic of boiling, and

2) a receiver hydrophone downstream from the boiling area to measure the attenuation of sound from an upstream input hydrophone as the sound passes through the boiling area. It was concluded that passive listening with a single internal hydrophone was not possible. The attenuation method demonstrated promise as a system of boiling detection, but it was recognized that major difficulties would be present with hydrophone design under the environment imposed by an operating reactor.

Boyd (49) was also active in the design of another nucleate boiling detection system. It was proposed to detect local nucleate boiling in the S3G reactor core by ion chambers inserted into thimbles which enter the core. Nucleate boiling detection in the system depended on the detection of fluctuations in the local thermal flux produced by nucleate boiling. Vapor bubbles cause a variation in the neutron moderator (H_2O) density, resulting in a corresponding variation in the local thermal flux which is detected by an ion chamber. By comparing the intensity of the portion of the frequency spectrum of the ion-chamber signal affected by nucleate boiling with a portion unaffected by boiling, an indication of boiling was obtained. An increase in the intensity of the former spectrum segment relative to the latter segment is an indication of boiling. A circuit was constructed to give a null reading when there is no boiling and

a deviation from the null signal when boiling occurs.

The system was designed to indicate the presence of boiling at 110% or less of the power level at which boiling begins. The desired sensitivity required 10^{12} to 10^{13} ionizing events in the ion-chamber per second in a flux of 10^{14} nv. In-pile and other experiments proved the feasibility of using the neutron sensitive ion-chamber to detect nucleate boiling in a reactor core (50).

Several papers describing impedance methods of transient void fraction measurements in water reactors were presented at the Symposium on In-Core-Instrumentation held June 15-20, 1964 in Oslo, Norway. The paper of Spigt et al. (51) is typical of the work relating to the impedance method. Results of void fraction measurements to determine the void fraction distribution along the height of a fuel channel are given. The impedance method is compared with the γ-ray attenuation technique, and Spigt concludes that the impedance method for void fraction determination gives reproducible and accurate results. It is further reported that the method opens the way to determine and to analyze in more detail, the phenomena associated with the statics and dynamics of two-phase flow systems.

Orbeck (52) and Björkman and Rundquist (53) both describe impedance-type void measuring instruments suitable for dynamic measurements in the core of boiling water reactors.

The technique of measurement is based upon the principle that the impedance between two plates immersed in a two-phase mixture will change as the void fraction changes. Measurements can be made of the electrical resistance or capacitance. The difference between the two measurements is mainly determined by the measuring frequency, which are around 3,000 cycles per second and 50 Mega-cycles per second respectively.

More recent work in this area has been done by Randall (54). Randall applied basic noise analysis techniques to an experimental demonstration of a conductivity cell cross-correlation method for measurement of flow rate and other operating parameters. The knowledge gained from work with a water loop is to be extended to use in liquid metal systems.

Actually, until recently only a minimal amount of work had been done on the problem of detecting boiling in a nuclear reactor. But with progress of the development program for fast sodium cooled reactors and the building of the High Flux Isotope Reactor, boiling detection has become more important. As a result the problem is now receiving more attention. The hostile temperature and radiation environment in a sodium cooled fast power reactor places even more demands on detection equipment and techniques.

Saxe (55) has recently presented a paper in which he surveys the methods of detecting boiling in nuclear reactors.

Several proposed methods of detection are evaluated and ranked in order of preference, after considering the phenomena which might provide a signal indicating boiling and the conditions under which the measurements would have to be made. He concluded that the preferred method was one based on ultrasonic energy and a technique based on neutron measurements was ranked second. An acoustical method also shows promise as a means of boiling detection in a reactor.

These methods will be discussed, but first a few other techniques which have exhibited some success in detecting boiling will be discussed.

The first of these is known as the "burst cartridge detection" system. Evans (56) has studied two classes of systems to detect a fault condition within a sub-assembly as fast as possible. The methods are for use as instrumentation in the United Kingdom's P.F.R. (protype fast reactor). The two classes of systems are an early-warning system which would detect local channel blockage conditions before any cladding has failed, and a clad-failure detection system which would operate in the shortest possible time.

The early-warning system's studied were thermal noise techniques and acoustic techniques. The burst cartridge detection (B.C.D.) system is based on the detection of fission product release and the depressurization of a fuel pin. The decision was made that, for the P.F.R., the principal

instrumentation systems will be B.C.D. backed up by boiling detection as an early-warning if the latter proves to be feasible.

If a fault is detected within the core, then it is very desirable to be able to locate the individual sub-assembly involved. At present, the only way proposed for doing this is to physically take samples of sodium from every sub-assembly.

The problem of using radioactive methods in a sodium cooled reactor like the P.F.R. is to distinguish the activity of the fission products from the gamma-rays of the sodium-24. Evans reports that this will be done by monitoring the sodium for the neutrons from fission fragments. This is similar to the proposed method for monitoring fuel-failure in the Fast Flux Test Facility. The detection time response is dominated by the transit time from the fault to the monitor. It is expected that it will be from 10 to 30 seconds; with the lower limit dictated by the hydraulic design of the reactor.

A continuing effort at Atomics International for investigating boiling liquid metals and two phase flow are described by Logan *et al.* (18). A development program for a reliable consistent method for detecting boiling in liquid metals is discussed.

Boiling was induced in a 1/8 inch annulus in a 1/2 inch inside diameter tube using external radiant heaters. A

permanent magnet flowmeter was used to monitor the sodium flow through the test section. Boiling sounds were detected with an accelerometer attached to the steel housing about 2 feet above the test section. The accelerometer and flowmeter signals were recorded on a portable FM magnetic tape system following amplification. Recordings were taken at various boiling and non-boiling conditions.

It was concluded from these tests that by measuring the signal intensity at particular frequencies, both the flow and accelerometer signals could be used to detect the onset of boiling. However, it was observed that the flow signal had a better signal to noise ratio than did the accelerometer signal. Also, the flowmeter exhibited a faster response time plus it was observed that almost any physical disturbance which created wide band noise, such as turning on a valve, rapping on the test section, etc., caused sound bursts electronically indistinguishable from the boiling sounds. Consequently, it was decided to use the flowmeter signal as a means for detecting boiling, so as to protect a high flux bayonet heater during further experiments with liquid sodium.

The analysis of coolant temperature fluctuations, i.e., thermal noise, as a means of boiling detection has received some attention at Argonne National Laboratory. Greebler (57) also reports that thermal noise is being investigated as a means of boiling detection at General Electric. Early work

in this area was done by Barclay and Ledwidge (58), who reported a noise bandwidth limited to frequencies less than about 1 cycle per second. In order to increase the frequency range, Barclay and Ledwidge are developing an eddy current probe.

Evans (56) reports on the use of thermal noise to detect faults in a sub-assembly of the Prototype Fast Reactor. He indicates that the average outlet temperature of a sub-assembly is very insensitive to local high temperature conditions within it, due to the finely divided nature of the sub-assembly and the large pressure drop across it. To overcome this insensitivity a new principle of outlet temperature monitoring has been investigated quantitatively. It depends on the fact that a local blockage, in present designs of fuel clusters, produces a corresponding change or "blip" in the radial temperature profile of the sodium which persists into the exit of the sub-assembly, although with some dispersion. The turbulent mixing of this hotter "blip" with its colder surroundings produces temperature fluctuations. The "blip" may then be detected at an appropriate location downstream by measuring statistically the strength of the temperature fluctuations. Evans reports that, for a selected band-width, this measurement of the root-mean-square temperature is generally about ten times more sensitive in detecting blockages than the more

conventional measurement of the mixed-mean temperature.

Three of the most important problem areas to be overcome in the instrumentation of a commercial sodium cooled fast breeder reactor are (59):

1. High integrity leads are required to bring the sensor signals out of the reactor vessel.
2. Reliable connectors are needed for the passage of signals through the reactor vessel.
3. The severe environmental effects of nuclear radiation, temperature, vibration and shock.

The several proposed methods of detecting boiling, plus other instrumentation, require several types of leads, each with different problems. For example, thermocouples and magnetic flowmeters will require well-insulated leads that do not introduce spurious differential mode potentials, even of the order of fractions of a millivolt. Turbine flowmeter leads must handle weak signals in the millivolt range.

The connector problem appears to be more severe than originally anticipated. The radiation damage and high temperature effects near the core give rise to very difficult problems. As a result, connections made under sodium will probably not really be made by "connectors" in the normal sense of the word, because they will likely be enclosed in a device that has been sealed by welding.

Connectors can be a source of signal error due to

leakage, thermal emf's, and signal distortions caused by capacitance and inductance effects of other conductors. Noise is also more readily picked up in them due to the discontinuity in their shielding.

The accuracy, lifetime and reliability of all in-core instrumentation is expected to suffer because of the high temperatures and radiation damage. At temperatures around 100-120^{o}F, the magnet in a permanent magnet flowmeter is expected to be in difficulty. How the magnet will respond with exposure to the fast neutron flux in a power reactor is still unknown and could be important. Also the magnitude of the false signals excited in the cable by the intense nuclear radiation is not known and may possibly be significant. The effects of mechanical shock and stray electrical fields is being investigated at Argonne National Laboratory (60).

The effect on coolant thermocouples of long exposure to fast neutrons is not known, and relatively little is known about the problems involving thermocouple response times versus exposure to the reactor environment. Another major problem encountered when employing thermocouples is providing adequate electrical insulation under the high temperatures and radiation fields present in a sodium cooled fast reactor.

In the face of many technical problems, some of which were briefly mentioned, there appears to be three main methods

of incipient boiling detection under investigation. These are 1) an acoustic method, 2) an ultrasonic method and 3) a neutron flux noise method.

B. Acoustic Method

The acoustic method currently receiving attention is based on listening for the acoustic emissions accompanying boiling. These acoustic signals cover a very wide range of frequencies and are not limited to those in the audible range. Acoustic emissions or "noises" manifest themselves in the form of pressure or mechanical waves.

There are many sources of noise associated with boiling. Noise is produced when bubbles are formed, collapse, or when their volume pulsates in such a way that a pressure wave is propagated. Noise is also produced when a bubble detaches itself from the heating surface. The boiling noise will then be characterized by a sum of the spectra from all these sources of acoustic emissions. Measurements by various investigators indicate that the noise has a wide-band "quasi white" spectrum with an unknown upper limit (61). (The term "white" spectrum refers to a spectrum in which all frequencies are equally present.)

There are many papers which deal with such mechanisms as bubble formation, growth, collapse and the generation pressure pulses (62, 32).

Lord Rayleigh (63) was the first to show that large instantaneous pressures are produced when the collapse of a bubble is limited only by inertia forces. Plesset (64) calculated the spectral distribution of sounds for bubbles forming and collapsing in an incompressible liquid. The growth of vapor bubbles in a superheated liquid has been investigated by both Forrester and Zuber (65) and Plesset and Zwick (66).

The noise produced by sodium vapor bubbles differs from that of bubbles containing some entrained gas. In the case of bubbles containing gas, the collapse is cushioned and discrete frequencies associated with the natural period of oscillation of the bubble may be present. Minnaert (67) derived an equation for the resonant frequency of a gas bubble, and Strasberg (68) has discussed gas bubbles as sources of sound in liquids. James (69) has performed experiments on the use of noise as an aid to reactor operation.

Considerable progress on the acoustic method has been made subsequent to the early work of Hogan and Boyd discussed above.

Columb and Binford (70) report using an underwater microphone to detect the noise produced by boiling at a system pressure of 30 psia. Furthermore, they report that if the background noise is not too great, the onset of boiling can be detected. However, the authors report that this

noise has a relatively small amplitude compared to the hydraulic noise.

Macleod (71), Schwartz and Siler (72), and Ledwidge (73) also report measurements indicating that boiling may be detected by noise sensors. It appears though, that the spectral content of the boiling noise is essentially a function of the boiler vessel. Clayton (74) has concluded, similarly, that acoustical peaks caused by vapor-bubble boiling noise can be ascribed to the geometry of the container. Furthermore, Clayton observes that the reliable detection of local nucleate boiling will depend on whether the signal induced by boiling can be differentiated from the background noises.

A. J. Walton has been active in the investigation of acoustic methods for detecting boiling in channels of the United Kingdom's sodium cooled Prototype Fast Reactor. His paper on sonic methods for boiling detection presents a rather complete treatment of the method and associated problems (75).

Walton performed experiments using a lead-barium-titanate transducer, and water as the liquid since the similarity between water and sodium is sufficiently close. Initial measurements of boiling noise in a model fast reactor sub-assembly revealed that many variables were present. This resulted in the decision to study the noise due to boiling at the surface of a pin and then investigate how this is

modified by the presence of the sub-assembly. Two results of this work are: 1) stable gas bubbles form when a liquid which contains gas is heated, and behave as resonators at discrete frequencies which vary inversely with their size, 2) boiling noise in a sub-assembly is modified by the organ pipe type of resonances which it produces.

The work also points out that the detection of boiling by an acoustic system depends on being able to detect the boiling signal above the background noise produced by pumps and coolant flow. Other noises, even from sources outside the reactor, may prove to be troublesome. Also, a transducer capable of successful operation while immersed in liquid sodium must be developed. Otherwise, a sound guide to transmit the signal from a high temperature region to a low temperature area may be necessary.

In addition, Walton remarks that location as well as detection of boiling may be difficult due to a combination of the effects of standing waves, and entrained gas bubbles which may act as absorbers or reflectors.

Barclay and Ledwidge (58) have been primarily concerned with the detection of nucleate boiling in liquid metal cooled reactors. In this work, detection is by conventional piezo-electric transducers mounted on to the end of a mechanical wave guide. The wave guide carries the signal from the high-temperature high-radiation area to the transducer which

is located away from the extreme environment. The authors report that noise emitted from flowing sodium exhibits about the same spectra as does noise from boiling sodium. The major problem, again appears to be in detecting the boiling noise in the presence of an uncertain background noise.

In order to avoid the necessity of a wave guide, Anderson et al., of Argonne National Laboratory, have been working on a high-temperature acoustic sensor (76). The authors are attempting to develop a piezo-electric hydrophone which will retain wide band frequency response and reasonably high sensitivity while operating immersed in sodium. Because of the high temperature of operation, lithium niobate, with a curie temperature of 1210^{o}C, was chosen as the piezo-electric material. The sensor is composed of a 1 cm^{2} lithium niobate crystal sandwiched between a stainless steel face plate and a stainless steel backing. The transducer has been calibrated in sodium using a radio-frequency generator and a PZT-4 crystal to produce an acoustic signal in the sodium.

Recent high temperature tests with the sensor immersed in sodium revealed that differential thermal expansion was a problem. As a result, the lithium niobate crystal was fractured. Corrective measures are now being taken to prevent this type of failure.

In summary, it appears that the detection of boiling by

acoustic measurements is feasible. However, the ability to detect boiling in a particular operating reactor installation will depend on being able to distinguish boiling noise in the presence of numerous sources of background noise. It is difficult to estimate or predict the characteristics of expected background noise in a commercial fast breeder reactor.

C. Ultrasonic Method

The application of ultrasonic energy is another possible means of detecting superheat and boiling in a sodium cooled fast reactor. The initial work in the area was directed toward instrumentation in boiling water reactors (77). The emphasis has since shifted to developing the technique for application in liquid metals.

Basically the method consists of measuring the ultrasonic power required to induce cavitation in the liquid metal. The acoustic power required to produce cavitation in the liquid decreases as the boiling condition is approached. The method takes simultaneous account of either a decrease in the system pressure or an increase in temperature, or both.

Aeroprojects Incorporated have performed many experiments under a development program for an incipient boiling detector based on the application of ultrasonic energy.

Kartluke (78) presents the results of this research along with a detailed description of the design and assembly of the instrumentation.

In the early designs of instrumentation for use in water, cavitation was detected in terms of characteristic broad-band or "white" noise (79). A barium titanate crystal affixed to an ultrasonic wave guide served to pick up the signals. These signals were then fed through an amplifier and tuned filter to a broad-band frequency analyzer. An oscilloscope then displayed a trace which exhibited frequency perturbations or "hash" in the presence of cavitation.

A typical display of this noise exhibited a high amplitude spike between 0 and 50,000 cycles per second, which represented a subharmonic of the driving frequency. It was the critical examination of this subharmonic response which led to the development of a more reliable and sensitive technique for detecting the onset of cavitation (80).

By acoustically driving a rod longitudinally, there is a resonant frequency corresponding to a standing-wave condition where the ends are free and two nodes occur in the rod. This is considered as the fundamental driving frequency, f_1, even though a standing-wave having one node and a frequency of $f_o = f_1/2$ is also a possible mode of vibration. It can be demonstrated theoretically that subharmonics cannot be excited by such a method, but the higher overtones

f_2, f_3, etc. will be present in the frequency spectrum of the response at the bar.

As a result, the frequency spectrum for such a system will ideally have distinct resonance peaks at frequencies determined by

$$f_i = \frac{n\ c}{2\ l} \tag{6}$$

where

i = mode index

c = velocity of sound in the rod

l = length of rod

n = 2,3,4,....

By placing the free end of this rod in a liquid and exciting the bar sonically at sufficient power, cavitation of the liquid will result. Since the cavities so produced will have a range of sizes and will collapse at different times during the acoustic pressure cycle, broad-band noise will be generated.

It is the interaction of this "white" noise with the rod that allows the detection of cavitation. Some of the broad band noise will occur at the frequency f_o, corresponding to subharmonic of the rod. This new frequency thus excited and its appearance can be taken to indicate the onset of cavitation.

Experiments at Aeroprojects have established that

this ultrasonic instrumentation is feasible for detecting incipient boiling in liquid metals. It is also reported that a multipoint ultrasonic boiling detection apparatus appears practical for use in a critical coolant channel.

An advantage of this system is that by means of a hermetically sealed isolation mount, the probe of the detector can penetrate the walls of vessels. These mounts are force-insensitive and allow all sensitive parts of the system to be located outside the high temperature and radiation fields.

The ultrasonic method is the only method which allows one to detect the approach to conditions conducive to boiling. All other methods rely on detecting signals excited after boiling has commenced. However, it suffers from the disadvantage of yielding information only about the liquid in the immediate vicinity of the probe. Since sodium cooled reactors are designed such that no boiling should occur anywhere in the reactor system, it will be the local boiling at unknown locations induced by unpredictable causes that the detection system must sense. Consequently, many probes would be required to protect the entire reactor from the occurrence of unknown boiling.

D. Neutron Noise Method

The third method of boiling detection which is currently receiving attention for use in sodium cooled reactors, is based on neutron flux measurements. That is, fluctuations of the neutron level about some time-average value, i.e., neutron noise, is the signal which is analyzed to gain an indication of the occurrence of boiling.

Moore (81, 82) was the first to suggest the use of neutron noise measurements to obtain information regarding an operating reactor. It was recognized that a zero power reactor, by virtue of the statistical variations in the neutron yield per fission, neutron leakage, and absorption processes, has an internal random driving function. Furthermore, it was suggested by Moore and later verified by Cohn (83), that the noise spectrum associated with these events is approximately white.

The presence of this inherent driving function means one does not have to be concerned with the problems of designing a system which will operate within the reactor and provide the driving function. This, plus the wide band characteristics of the driving function, makes it theoretically possible to consider all frequencies simultaneously. If it were possible to derive the necessary information from neutron detectors placed outside the reactor vessel, the ideal method would be

at hand. However, Cohn (84) has shown that the detector efficiency must be at least 5×10^{-5} if the measurements of neutron noise are to yield meaningful results. In most cases this necessitates placing the detectors close to the core, and hence inside the pressure vessel.

Under normal operating conditions, the neutron flux noise will possess definite frequency characteristics. When boiling occurs, bubbles will form and collapse and their space and time dependence will affect the local absorption rate, leakage, slowing down, etc., and hence will affect the neutron level. Under the influence of these boiling induced perturbations, the neutron flux noise may exhibit frequency characteristics which differ from those under normal non-boiling conditions. This then serves as the basis for boiling detection by neutron noise measurements.

Although the early work by Boyd (49, 50) described above did not employ noise measurements per se, his work did show that boiling could be detected by neutron flux measurements. The method described by Boyd employed the fact that the boiling induced fluctuations in the neutron flux were low frequency (25-60 cycles per second) phenomena, whereas the high frequency neutron-noise was unaffected by the boiling.

Early neutron noise measurements for the purpose of boiling detection in a water cooled reactor were made by Columb and Binford (70) at Oak Ridge National Laboratory.

An ionization-chamber placed in one of the standard chamber locations close to the core provided the signal. The current output from the chamber was converted to a voltage by means of a 1 mega-ohm resistor, and then amplified by an A.C. coupled amplified with a gain of 100 and a flat frequency response from 0.1 to 1,000 cycles per second. The amplified signal was then recorded on a tape recorder and digitalized for input into a 7090 IBM computer.

Four ten-second observations taken with and without boiling were analyzed. Both the auto-correlation functions and the spectral densities indicated a difference between the samples with boiling and those without boiling. The standard deviation of the auto-correlation function curves was 22%, that of the spectral density functions was 45%. The authors concluded that the method could be used to detect boiling and that the auto-correlation function would yield the information more rapidly than the spectral density.

Fry et al. (85) measured the neutron power spectral density in an effort to detect the onset of nucleate boiling in the ORR. Neutron excited fluctuations in an ion chamber during a boiling experiment were analyzed to determine if any boiling related noise could be detected. The results indicated that the shape and spectra were extremely dependent on the coolant flow rate. Thus the

authors concluded that the effects of boiling on the neutron power spectral density would likely be masked by these coolant induced neutron fluctuations.

Yamada and Kage (86) have also discussed the effects of coolant flow as a source of reactor noise which could interfere with the detection of boiling.

Neutron noise measurements at the Enrico Fermi plant by Rajagopal (87) reportedly exhibited two pronounced resonances between 10 and 15 cycles per second which were attributed to nucleate boiling. These measurements were made using an ion-chamber located outside of the reactor core. Similar results were reported by Rajagopal (88) for measurements at the Saxton and Yankee reactors.

Further measurements by Rajagopal and Gallagher (89) at the Saxton reactor, exhibited a sharp distinct resonance in the neutron power-spectral-density curve at 16 cycles per second. It is reported that investigations of the peak under various operating conditions demonstrated that it was definitely related to nucleate boiling.

Jordan (90) describes an experiment in which a specially instrumented fuel assembly of the 3 MW GTR (Ground Test Reactor) was orificed to reduce the flow from 1.8 to 0.6 feet per second. Boiling was predicted to occur at a reactor power level of 2.2 Mega-watts. Power spectral density analysis of an ion-chamber signal yielded reliable detection of

boiling for a void fraction of 0.014 $\Delta V/V$ per element. The first indication of boiling came from thermo-couple and the ion-chamber response at a power level of 2.35 MW.

The author presents power spectral density curves which exhibit a distinct multiple peak structure over the frequency range 0.3 to 2.5 cycles per second. The peak of largest magnitude occurred at 0.3 cycles per second with the following peaks becoming successively smaller in amplitude. At a lower power level these peaks disappeared.

Jordan reports that the GTR period trip provided useful protection against boiling, but the detection sensitivity was less than one-tenth that of the power spectral density analysis.

In this experiment it was observed that due to the relatively short void lifetime (0.2 sec) in the subcooled water, and a low frequency of occurrence (0.33/sec), there was no continuous change in the reactivity due to the voids. The reactor reportedly responded to each void individually as a power fluctuation and did not rise above the non-boiling power trace.

Mulcahey (91) has reported that work has recently begun at Argonne National Laboratory in an effort to ascertain whether neutron noise measurements are feasible as a method for the detection of boiling in sodium cooled reactors. Fry and Robinson (92) have done a considerable amount of

work in the field of neutron flux noise measurements. In particular, the authors have been active in investigating the use of neutron density fluctuations as a reactor diagnostic tool. They have performed numerous neutron flux noise analysis at two Oak Ridge National Laboratory reactors. These were the High Flux Isotope Reactor (HFIR) and the Molten-Salt Reactor Experiment (MSRE).

Over 150 spectra representing 15 fuel cycles were measured at the HFIR. These spectra were recorded so they could become part of a collection, or library, of neutron flux noise measurements which could then be used in diagnosing unexpected and abnormal reactivity behavior in the HFIR. Measurement of the relative amount of entrained helium gas in the fuel salt, by neutron noise analysis, was the main objective at the MSRE.

In one instance, the authors' had recorded the output from an ion-chamber for several days without analyzing the measurements. Upon completion of the fuel cycle, examination of the control rods revealed that the upper guide bearing on one of the shim-safety plates had failed. Subsequent analysis of the noise measurements show a distinct peak, not previously observed, in the spectra at 5 cycles per second. It is interesting to note that the operating personnel had not observed any indication of unusual behavior during this time. During a later fuel cycle, the rod bearing failed

again, and noise analysis showed there was a peak in the spectra at 5 cycles per second similar to the one observed previously.

These authors have also compared the gamma spectrum with the neutron spectrum obtained at the same time. These measurements indicated that the prompt-gamma spectrum has the same shape as the neutron spectrum. This might prove useful when it is desirable to place the detectors outside the pressure vessel where the neutron signal would be attenuated, but where the demands on instrumentation are lessened.

Fry and Robinson conclude that neutron noise analysis can be a very useful reactor diagnostic tool, especially when employed with on-line computers. However, they report that the usefulness of the method depends to a large extent on the availability of a reference library of normal spectra and abnormal spectra, corresponding to known causes, in order to recognize similar anomolies.

From the work discussed above, it appears that if the neutron noise induced by the boiling of sodium is of sufficient magnitude and is characterized by some low frequency spectra, then neutron noise measurements are a feasible means of boiling detection. However, once more there is the question of the relative magnitude of the boiling induced noise and the background neutron flux noise, including the effect of coolant flow induced noise.

IV. THEORY

The analytical study to be presented in this dissertation will, for the sake of clarity, be very briefly outlined before the details of the theory are presented.

From noise theory the following relationship is known to hold (93)

$$\Phi_{yy}(w) = |G(jw)|^2 \Phi_{xx}(w) \tag{7}$$

where

$x(t)$ = input driving function

$y(t)$ = output of system

$X(s)$ = Laplace transform of $x(t)$

$Y(s)$ = Laplace transform of $y(t)$

$G(s)$ = transfer function of system

$$= \frac{Y(s)}{X(s)}$$

$\Phi(w)$ = spectral density of function

$|\ |^2$ = magnitude squared.

Knowing the transfer function, G, and the spectral density of the input function, Φ_{xx}, one can calculate the spectral density of the output, Φ_{yy}. If G is the transfer function of a nuclear reactor and Φ_{xx} the spectral density of some reactivity perturbation, then the neutron flux spectral density, Φ_{yy}, can be determined.

By simulating the normal operating conditions of the reactor by an appropriate input spectral density, Φ_{xx}, such as a white spectrum, the normal output flux spectral density can be calculated. This then can be compared with the results obtained by postulating some Φ_{xx} which contains frequency characteristics of boiling sodium. Consequently, this comparison would allow one to make implications regarding the detection of boiling.

A. Natural Mode Analysis

For large reactors, such as the 1000 MWe sodium cooled fast breeders being designed today, space independent or "point" reactor kinetic equations are not generally adequate to describe the neutronics of the system. Especially when the system is excited by spatially localized perturbation. There are many instances where the distortion of the spatial shape of the flux during transient conditions is very significant (94, 95). Thus one must deal with the more complicated space and time dependent reactor equations.

In attempting to solve the space-time neutron equations one normally trys to separate the equations into space equations and time equations. Three methods which have been proposed to accomplish this separation are: nodal analysis, the instantaneous tilt method, and modal analysis (94). The modal analysis method will be employed in this work.

The modal analysis technique represents the neutron fluxes and other dependent variables, e.g. precursor concentration, by a finite linear combination of space-dependent basis vectors with time-dependent coefficients of combination. This representation reduces the space-time problem to a selection of basis vectors, or space modes, and determination of the time-coefficients of combination. The specific procedure followed depends on the choice of base vectors. The so-called "Natural Modes" of the reactor will be utilized as the basis vectors for the analysis here. The approximate solution for the flux and other dependent variables is then said to be the natural mode approximation (96, 97).

Multi-group diffusion theory approximations enable the space and time dependent behavior of a nuclear reactor without feedback or external sources to be described by the matrix equation (96)

$$L(\vec{r},t)\vec{\Phi}(\vec{r},t) = \frac{\partial\vec{\Phi}(\vec{r},t)}{\partial t} \quad , \tag{8}$$

where

$\vec{\Phi}(\vec{r},t) = \text{col}[\phi_1,\phi_2,\ldots\phi_G,C_1,C_2,\ldots C_P]$

ϕ_g = group g neutron flux

C_p = group p delayed neutron precursor

G = number of neutron flux groups

P = number of precursors.

The matrix operator $L(\vec{r},t)$ includes all the production and loss operators and is of dimension K x K, where K = G + P.

The Natural Mode Approximation (NMA) is a method for solving Equation 8 by representing the solution as a finite sum

$$\vec{\Phi}(\vec{r},t) \cong \sum_{m=1}^{M} \sum_{k=1}^{K} A_{mk}(t)\vec{\psi}_{mk}(\vec{r}) \quad . \tag{9}$$

That is, $\vec{\Phi}$ is represented as a finite sum of products of time dependent coefficients, $A_{mk}(t)$, and space dependent functions, or base vectors, $\vec{\psi}(\vec{r},t)$. It is assumed that the $\vec{\psi}_{mk}$'s satisfy the same homogeneous boundary conditions as $\vec{\Phi}$.

The NMA method considers the critical or steady-state reference condition defined by

$$L_o\vec{\Phi} = 0 \quad , \tag{10}$$

where L_o represents the steady-state matrix operator. The base vectors, $\vec{\psi}_{mk}(\vec{r})$, are obtained as the "spatial eigenvectors" of the eigenvalue problem

$$L_o\vec{\psi}_{mk}(\vec{r}) = \lambda_{mk}\vec{\psi}_{mk}(\vec{r}) \quad . \tag{11}$$

The solutions of this equation are then the so-called "Natural Modes" of the reactor. Note that in this case the

eigenvector is a space-dependent function and not merely a scaler. Hence the name "spatial eigenvector" will be used in this work. Here m is the mode index and k is the eigenvalue index.

The spatial eigenvector is composed of an amplitude vector, $\vec{e}_{mk}$, times a space dependent vector $\vec{S}_{mk}(\vec{r})$. For the case of a bare reactor the spatial dependence of $\psi^{i}_{mk}(\vec{r})$ is the same for all i. Thus $\vec{S}_{mk}$ can be represented as a scaler function $S_{mk}(\vec{r})$. Using this notation and for a bare reactor, one can write the vector $\vec{\psi}_{mk}(\vec{r})$ as

$$\vec{\psi}_{mk}(\vec{r}) = \text{col}[\psi^{1}_{mk}(\vec{r})\ \psi^{2}_{mk}(\vec{r})\ \ldots\ \psi^{3}_{mk}]$$

$$= \vec{e}_{mk}\ S_{m}(\vec{r})$$

$$= S_{m}(\vec{r}) \begin{bmatrix} e^{1}_{mk} \\ e^{2}_{mk} \\ \cdot \\ \cdot \\ \cdot \\ e^{K}_{mk} \end{bmatrix} . \qquad (12)$$

For each mode specified by m and each eigenvalue specified by index k, there is an eigenvector $\vec{e}_{mk}$ with K elements. The space function $S_{m}(\vec{r})$ dependents only on the mode and is independent of the eigenvalues corresponding to that mode.

At this point, the subscript notation used in the NMA

merits some clarifying comments. The mode index is necessary because the steady state matrix operator, L_o, contains operators which are dependent on the mode. In particular, L_o will include the Laplacian operator ∇^2. From the First Fundamental Theorem of Reactor Theory (98), which is valid for the bare reactor model considered in this work, it can be concluded that

$$\nabla^2 \phi_g + B^2 \phi_g = 0$$

or

$$\nabla^2 \phi_g = -B^2 \phi_g \quad , \tag{13}$$

where B^2 is the buckling. But in general B^2 is a function of the mode. For example, consider a rectangular coordinate system, then one has operationally

$$\nabla^2 = -B^2_{\ell mn}$$

$$= -\left[\left(\frac{\ell \pi}{a}\right)^2 + \left(\frac{m\pi}{b}\right)^2 = \left(\frac{n\pi}{c}\right)^2 \right] \quad . \tag{14}$$

By making the substitution of Equation 14 for ∇^2 in the matrix operator L_o, it then follows that L_o is a function of the mode. It follows that ∇^2 and hence L_o then require three indices (e.g. ℓ, m, and n) to completely specify the mode for a three dimensional problem. Consequently the eigenvalue problem requires four subscripts,

$$[L_o]_{\ell mn}\vec{\psi}_{\ell mnk}(x,y,z) = \lambda_{\ell mnk}\vec{\psi}_{\ell mnk}(x,y,z) \quad . \tag{15}$$

The fourth subscript, k, is the eigenvalue index. For each mode specified by ℓ, m, and n, there will be K eigenvalues determined by Equation 11. Thus k runs from 1 to K for each mode.

It is easy to show that the equation which determines the eigenvalues is

$$\det[[L_o]_{\ell mn} - \lambda_{\ell mnk}[I]] = 0 \quad , \tag{16}$$

where [I] is the identity matrix and the R.H.S. of Equation 14 was substituted into L_o for ∇^2. Note that the eigenvalues are not directly dependent upon the form of the space modes.

In view of Equations 13 and 14 and the previous statement that the spatial eigenvectors satisfy the same homogeneous boundary conditions as Φ, one can conclude that[1]

$$\nabla^2\vec{\psi}_{Mk}(x,y,z) = -B_M^2\,\vec{\psi}_{Mk}(x,y,z) \quad . \tag{17}$$

From this, one can conclude that for a given mode (i.e. ℓ, m, and n specified) each element of the vector $\vec{\psi}_{Mk}$ has the same spatial "shape" determined by Equation 17. This equation then determines the space functions, $S_M(x,y,z)$. Although each element has the same space function, $\vec{\psi}_{Mk}$ must

---

[1] To make the subscript notation less cumbersome M is used to denote the mode indices ℓ, m, and n.

also satisfy Equation 15. Equation 14 is equivalent to K simultaneous equations and will determine the relative amplitudes of the elements of $\vec{\psi}_{Mk}$. Note that since B^2 depends only on M, the space functions for $\vec{\psi}_{M1}, \vec{\psi}_{M2}, \ldots \vec{\psi}_{MK}$ will all be identical. But for each value of k the relative amplitudes will vary.

For sake of definitness, consider a one-dimensional model with one energy group and one delayed neutron group. Equation 17 would yield

$$\vec{\psi}_{Mk}(x) = \begin{bmatrix} \psi^1_{Mk} \\ \psi^2_{Mk} \\ \psi^3_{Mk} \end{bmatrix}$$

$$= \begin{bmatrix} e_1 \sin B_M x \\ e_2 \sin B_M x \\ e_3 \sin B_M x \end{bmatrix} , \qquad (18)$$

where e_1, e_2, and e_3 are the amplitudes to be determined. Substituting this solution into Equation 15 yields

$$[L_o]_M \begin{bmatrix} e_1 \sin B_M x \\ e_2 \sin B_M x \\ e_3 \sin B_M x \end{bmatrix} = \lambda_{Mk} \begin{bmatrix} e_1 \sin B_M x \\ e_2 \sin B_M x \\ e_3 \sin B_M x \end{bmatrix} , \qquad (19)$$

or

$$[L_o]_M \sin B_M x \begin{bmatrix} e_1 \\ e_2 \\ e_3 \end{bmatrix} = \lambda_M \sin B_M x \begin{bmatrix} e_1 \\ e_2 \\ e_3 \end{bmatrix} \quad . \tag{20}$$

Obviously the factor $\sin(B_M x)$ can be cancelled from both sides of Equation 20, and one is left with the conventional eigenvalue problem

$$L_o \vec{e} = \lambda \vec{e} \quad . \tag{21}$$

Thus the L_o matrix yields the eigenvalues, λ_{Mk}; and the corresponding eigenvectors represent the relative amplitudes of the solutions.

To complete the analysis, the time dependent coefficients, $A_{Mk}(t)$, must be determined. This is accomplished by application of an orthogonality relationship.

The spatial eigenvectors of Equation 11 and those of the adjoint equation

$$L_o^T \vec{\psi}^*_{Qj}(x,y,z) = \lambda^*_{Qj} \vec{\psi}^*_{Qj}(x,y,z) \quad , \tag{22}$$

where L_o^T is the transpose of L_o, have a very useful orthogonality property if $\vec{\psi}_{Mk}$ and $\vec{\psi}_{Qj}$ satisfy the same homogeneous boundary conditions. This orthogonality property is (99, 100)

$$\langle \vec{\psi}^{*}_{Qj}, \vec{\psi}_{Mk} \rangle = 0 \quad \text{for} \quad \lambda_{Mk} \neq \lambda_{Qj} \quad , \tag{23}$$

where

$$\langle \vec{X}, \vec{Y} \rangle \equiv \text{inner product}$$

$$= \int_{\text{reactor}} \vec{X}^{T} \vec{Y} \, dV \quad . \tag{24}$$

This results from the assumption that the eigenvalues, λ_{Mk}, are distinct. Furthermore it will be assumed that

$$\langle \vec{\psi}^{*}_{Mk}, \vec{\psi}_{Mk} \rangle \neq 0 \tag{25}$$

which implies that the eigenvalues λ^{*}_{Mk} are the same as λ_{Mk}.

Substituting Equation 9, for $\Phi(x,y,z,t)$, into Equation 7 yields

$$\frac{\partial}{\partial t} \sum_{M} \sum_{K} A_{MK}(t) \vec{\psi}_{MK}(x,y,z) = L \sum_{M} \sum_{K} A_{MK}(t) \vec{\psi}_{MK}(x,y,z) \quad . \tag{26}$$

Now multiply this equation by $\vec{\psi}^{+}_{Qj}$ and integrate over the reactor to obtain on the L.H.S.

$$\int_{\text{reactor}} \int \int \{ \frac{\partial}{\partial t} \sum_{M} \sum_{K} A_{MK}(t) \vec{\psi}^{+}_{Qj} \vec{\psi}_{MK} \} dV \quad . \tag{27}$$

Since the integration is over space, and not time, this can be rewritten as

$$\frac{\partial}{\partial t}\sum_M\sum_K A_{MK}(t)\iiint_{\text{reactor}}\vec{\psi}^{+}_{Qj}\vec{\psi}_{MK}dV = \frac{\partial}{\partial t}\sum_M\sum_K A_{MK}(t)\langle\vec{\psi}^{+}_{Qj},\vec{\psi}_{MK}\rangle \quad . \quad (28)$$

From the orthogonality relationship of Equation 23 one can see that the inner product term in the double summation will be zero except when M = Q and K = j, thus the L.H.S. of Equation 26 becomes simply

$$\frac{\partial}{\partial t} A_{Qj}(t)\langle\vec{\psi}^{+}_{Qj},\vec{\psi}_{Qj}\rangle \quad . \quad (29)$$

Now on the R.H.S. of Equation 26 add and subtract

$$\sum_M\sum_K L_o\, A_{MK}\vec{\psi}_{MK}$$

before multiplying by $\vec{\psi}^{+}_{Qj}$ and integrating. That is, first write

$$\sum_M\sum_K L\, A_{MK}(t)\vec{\psi}_{MK}(x,y,z) = \sum_M\sum_K(L-L_o)A_{MK}(t)\vec{\psi}_{MK} + \sum_M\sum_K L_o A_{MK}\vec{\psi}_{MK} \quad . \quad (30)$$

Then multiply by $\vec{\psi}^{+}_{Qj}$ and integrate over the reactor to obtain

$$\sum_M\sum_K\langle\vec{\psi}^{+}_{Qj}(L-L_o)A_{MK}(t)\vec{\psi}_{MK}\rangle + \sum_M\sum_K\langle\vec{\psi}^{+}_{Qj},L_o A_{MK}\vec{\psi}_{MK}\rangle \quad . \quad (31)$$

The second term of Equation 24 can be simplified by noting that L_o does not operate on $A_{MK}(t)$, and from Equation 11 that $L_o\vec{\psi}_{MK} = \lambda_{MK}\vec{\psi}_{MK}$. Thus

$$\sum_M \sum_K \langle \vec{\psi}^+_{Qj}, L_o A_{MK} \vec{\psi}_{MK} \rangle = \sum_M \sum_K \langle \vec{\psi}^+_{Qj}, L_o \vec{\psi}_{MK} \rangle A_{MK}$$

$$= \sum_M \sum_K \langle \vec{\psi}^+_{Qj}, \lambda_{MK} \vec{\psi}_{MK} \rangle A_{MK}$$

$$= \sum_M \sum_K \lambda_{MK} \langle \vec{\psi}^+_{Qj}, \vec{\psi}_{MK} \rangle A_{MK} \quad . \tag{32}$$

Applying the orthogonality property once more leaves simply

$$\lambda_{Qj} \langle \vec{\psi}^+_{Qj}, \vec{\psi}_{Qj} \rangle A_{Qj} \quad , \tag{33}$$

as the second term in Equation 31. Combining the results of Equations 29, 31, and 33 it is seen that the relationship of Equation 26 has become

$$\frac{d}{dt} A_{Qj} \langle \vec{\psi}^+_{Qj}, \vec{\psi}_{Qj} \rangle = \lambda_{Qj} \langle \vec{\psi}^+_{Qj}, \vec{\psi}_{Qj} \rangle A_{Qj}$$

$$+ \sum \sum \langle \vec{\psi}^+_{Qj}, (1 - L_o) \bar{A}_{MK} \vec{\psi}_{MK} \rangle \tag{34}$$

or

$$\frac{dA_{Qj}}{dt} = \lambda_{Qj} A_{Qj} + \sum_M \sum_K \langle \vec{\psi}^+_{Qj}, (L - L_o) \vec{\psi}_{MK} \rangle A_{MK} / \langle \vec{\psi}^+_{Qj}, \vec{\psi}_{Qj} \rangle \quad . \tag{35}$$

There are (M·K) equations of the form of Equation 35. Because of the term,

$$\sum_M \sum_K \langle \vec{\psi}^+_{Qj}, (L - L_o) \vec{\psi}_{MK} \rangle A_{MK}$$

The equations are coupled and must be solved simultaneously. Much effort is required to obtain the time dependent coefficients due to this coupling.

One of the advantageous characteristics possessed by the natural mode expansion is the property of finality (101, 102). For expansions displaying finality, each time dependent coefficient is found separately as the solution of a single ordinary differential equation. If the expansion does not have the finality property, then it is necessary to solve N simultaneous equations for the N coefficients. It is from equating the property of finality with "naturalness" that the natural modes derive their name (101).

To illustrate the utility of the finality property in uncoupling equations such as 35, the kinetics equations are first written as

$$L\vec{\Phi} = (L_o + L_1)\vec{\Phi} = \dot{\vec{\Phi}} \quad . \tag{36}$$

or

$$L_o\vec{\Phi} = \dot{\vec{\Phi}} - L_1\vec{\Phi} \quad , \tag{37}$$

where the matrix operator, L, has been written as the sum of a steady state operator, L_o, and a perturbation operator, L_1. Forming the inner product of Equation 37 with $\vec{\psi}^{+}_{Qj}$ yields

$$\langle\vec{\psi}^{+}_{Qj}, L_o\vec{\Phi}\rangle = \langle\vec{\psi}^{+}_{Qj}, \dot{\vec{\Phi}}\rangle - \langle\vec{\psi}^{+}_{Qj}, L_1\vec{\Phi}\rangle \quad . \tag{38}$$

It can be shown that,

$$\langle \vec{\psi}^{+}_{Qj}, L_o \vec{\psi}_{MK} \rangle = \langle \vec{\psi}_{MK}, L_o^T \vec{\psi}^{+}_{Qj} \rangle \quad , \tag{39}$$

if $\vec{\psi}^{+}_{Qj}$ and $\vec{\psi}_{MK}$ satisfy the same vanishing boundary conditions. Thus since $\vec{\psi}^{+}_{Qj}$ and $\vec{\Phi}$ satisfy the same boundary conditions,

$$\begin{aligned} \langle \vec{\psi}^{+}_{Qj}, L_o \vec{\Phi} \rangle &= \langle \vec{\Phi}, L_o^T \vec{\psi}^{+}_{Qj} \rangle \\ &= \langle \vec{\Phi}, \lambda_{Qj} \vec{\psi}^{+}_{Qj} \rangle \\ &= \lambda_{Qj} \langle \vec{\Phi}, \vec{\psi}^{+}_{Qj} \rangle \quad . \end{aligned} \tag{40}$$

Now noting that $\vec{\Phi}$ and $\vec{\psi}^{+}_{Qj}$ commute, and substituting Equation 10, for the flux, into the R.H.S. of Equation 40 yields

$$\lambda_{Qj} \langle \vec{\Phi}, \vec{\psi}^{+}_{Qj} \rangle = \lambda_{Qj} \langle \vec{\psi}^{+}_{Qj}, \sum_M \sum_K A_{MK} \vec{\psi}_{MK} \rangle \quad . \tag{41}$$

Noting the orthogonality relation this reduces to

$$\lambda_{Qj} A_{Qj} \langle \vec{\psi}^{+}_{Qj}, \vec{\psi}_{Qj} \rangle \quad . \tag{42}$$

Thus Equation 38 becomes

$$\begin{aligned} \lambda_{Qj} A_{Qj} \langle \vec{\psi}^{+}_{Qj}, \vec{\psi}_{Qj} \rangle &= \langle \vec{\psi}^{+}_{Qj}, \frac{\partial}{\partial t} \sum_{MK} \sum A_{MK} \psi_{MK} \rangle - \langle \vec{\psi}^{+}_{Qj}, L_1 \vec{\Phi} \rangle \\ &= \frac{d}{dt} A_{Qj} \langle \vec{\psi}^{+}_{Qj}, \vec{\psi}_{Qj} \rangle - \langle \vec{\psi}^{+}_{Qj}, L_1 \vec{\Phi} \rangle \end{aligned} \tag{43}$$

when the orthogonality condition is applied. Now for small

perturbations it is assumed that $L_1\Phi \simeq L_1\Phi_o$, where Φ_o is the steady state solution. Solving Equation 43 for A_{Qj} yields

$$\frac{d}{dt} A_{Qj} = \lambda_{Qj} A_{Qj} + \langle \vec{\psi}^+_{Qj}, L_1 \vec{\Phi}_o \rangle / \langle \vec{\psi}^+_{Qj}, \vec{\psi}_{Qj} \rangle \quad . \tag{44}$$

The Equations 35 have thus been uncoupled, and now a simple system of differential equations can be used to determine the time coefficients, A_{Qj}.

B. Space Dependent Noise Theory

The space dependent noise formulation employed here, follows from a paper by Danofsky (103).

As seen earlier, the flux for a given energy group can be expressed in a modal analysis form as

$$\phi(x,y,z,t) = \sum_{\ell=1}^{M} \sum_{m=1}^{M} \sum_{n=1}^{M} \sum_{k=1}^{K} A_{\ell mnk}(t)\psi_{\ell mnk}(x,y,z) \quad . \tag{45}$$

Expressing $\phi(x,y,z,t)$ as a steady state or average flux plus a small time dependent component

$$\phi(x,y,z,t) = \phi_o(x,y,z) + \Delta\phi(x,y,z,t)$$

$$= \phi_o(x,y,z) + \sum_{\ell=1}^{M} \sum_{m=1}^{M} \sum_{n=1}^{M} \sum_{k=1}^{K} \Delta A_{\ell mnk}(t)\psi_{\ell mnk}(x,y,z) \tag{46}$$

For the noise formulation considered here, the time dependent

component will be assumed to have a zero average value. Next the correlation function (103, 104, 105) is formed[1]

$$\overline{\Delta\phi(\vec{r}_1,t)\Delta\phi(\vec{r}_2,t+\tau)}$$

$$= \overline{\sum_{mn}^{M}\sum_{k}^{K}\Delta A_{mnk}(t)\psi_{mnk}(\vec{r}_1)\sum_{uvw}^{M}\sum_{s}^{K}\Delta A_{uvws}(t+\tau)\psi_{uvws}(\vec{r}_2)} \tag{47}$$

It is significant to note that in this development there is no assumption that $\Delta\phi(\vec{r}_i,t)$ is of the same energy group as $\Delta\phi(\vec{r}_j,t+\tau)$. Thus cross correlation between space points and energy groups is very simple. The above equation can yield

$$\overline{\Delta\phi(\vec{r}_1E_1,t)\Delta\phi(\vec{r}_2,E_2t+r)}$$

$$= \sum_{mn}^{M}\sum_{k}^{K}\sum_{uvw}^{M}\sum_{k}^{K}\overline{\Delta A_{mnk}(t)\Delta A_{uvws}(t+\tau)}\,\psi_{mnk}(\vec{r}_1,E_1)\psi_{uvws}(\vec{r}_2,E_2)$$

$$\equiv \Phi_{\phi\phi}(\vec{r},\vec{r}_2,E_1,E_2,\tau) \quad . \tag{48}$$

To see that Equation 48 follows from Equation 47 expand the first few terms of Equation 47, without the time averaging,

---

[1]The vector $\vec{r}$ is used to specify the point (x,y,z), and the overbar denotes the time average.

$$\Delta\phi(\vec{r}_1,t)\Delta\phi(\vec{r}_2,t+\tau) = [\Delta A_{1111}\psi_{1111} + \Delta A_{1112}\psi_{1112} + \Delta A_{1113}\psi_{1113}$$

$$+ \Delta A_{1121}\psi_{1121} + \Delta A_{1122}\psi_{1122} + \Delta A_{1123}\psi_{1123} + \Delta A_{1131}\psi_{1131}$$

$$+ \cdots + \Delta A_{MMM1}\psi_{MMM1} + \Delta A_{MMM2}\psi_{MMM2} + \Delta A_{MMM3}\psi_{MMM3}]$$

$$[\Delta A_{1111}\psi_{1111} + \Delta A_{1112}\psi_{1112} + \Delta A_{1113}\psi_{1113} + \Delta A_{1121}\psi_{1121}$$

$$+ \Delta A_{1122}\psi_{1122} + \Delta A_{1123}\psi_{1123} + \Delta A_{1131}\psi_{1131} + \cdots$$

$$+ \Delta A_{MMM1}\psi_{MMM1} + \Delta A_{MMM2}\psi_{MMM2} + \Delta A_{MMM3}\psi_{MMM3}] \quad , \qquad (49)$$

or

$$\Delta\phi(\vec{r}_1,t)\Delta\phi(\vec{r}_2,t+\tau) = \Delta A_{1111}\Delta A_{1111}\psi_{1111}\psi_{1111}$$

$$+ \Delta A_{1111}\Delta A_{1112}\psi_{1111}\psi_{1112} + \Delta A_{1111}\Delta A_{1113}\psi_{1111}\psi_{1113}$$

$$+ \Delta A_{1111}\Delta A_{1121}\psi_{1111}\psi_{1121} + \cdots + \Delta A_{1111}\Delta A_{MMM1}\psi_{1111}\psi_{MMM1}$$

$$+ \Delta A_{1111}\Delta A_{MMM2}\psi_{1111}\psi_{MMM2} + \Delta A_{1111}\Delta A_{MMM3}\psi_{1111}\psi_{MMM3}$$

$$+ \Delta A_{1112}\Delta A_{1111}\psi_{1112}\psi_{1111} + \Delta A_{1112}\Delta A_{1112}\psi_{1112}\psi_{1112}$$

$$+ \Delta A_{1112}\Delta A_{1113}\psi_{1112}\psi_{1113} + \cdots + \Delta A_{MMM1}\Delta A_{1111}\psi_{MMM1}\psi_{1111}$$

$$+ \cdots + \Delta A_{MMM3}\Delta A_{MMM3}\psi_{MMM3}\psi_{MMM3} \quad . \qquad (50)$$

This can be written as

$$\sum_{mn}^{M}\sum_{k}^{K}\sum_{uvw}^{M}\sum_{s}^{K} \Delta A_{mnk}(t)\Delta A_{uvws}(t+\tau)\psi_{mnk}(\vec{r}_1,E_1)\psi_{uvws}(\vec{r}_2,E_2)$$

$$= \Delta\phi(\vec{r}_1,t)\Delta\phi(\vec{r}_2 t+\tau) \quad . \tag{51}$$

Next, take the time average in order to obtain Equation 48. Note that if $\vec{r}_1 = \vec{r}_2$ an auto-correlation function is obtained and if $\vec{r}_1 \neq \vec{r}_2$ a cross-correlation function is obtained. By defining the following

$$\Gamma_{mnk,uvws}(\tau) = \overline{\Delta A_{mnk}(t)\Delta A_{uvws}(t+\tau)} \quad , \tag{52}$$

Equation 48 can be written as

$$\Phi_{\phi\phi}(\vec{r}_1,\vec{r}_2,E_1,E_2,\tau)$$

$$= \sum_{mn}^{M}\sum_{k}^{K}\sum_{uvw}^{M}\sum_{s}^{K} \Gamma_{mnkuvws}(\tau)\ \psi_{mnk}(\vec{r}_1,E_1)\psi_{uvws}(\vec{r}_2,E_2) \quad . \tag{53}$$

To obtain the frequency domain equivalent of Equation 53 Fourier transform both sides of the equation to obtain

$$\hat{\Phi}(\vec{r}_1,\vec{r}_2,E_1,E_2,w)$$

$$= \sum_{mn}^{M}\sum_{k}^{K}\sum_{uvw}^{M}\sum_{s}^{K} \hat{\Gamma}_{mnkuvws}(w)\psi_{mnk}(\vec{r}_1,E_1)\psi_{uvws}(\vec{r}_2,E_2) \tag{54}$$

Thus we see that the problem of obtaining the space dependent

auto- or cross-spectral density (93) requires information on the cross spectral densities between time coefficients. These are easy to obtain in some cases.

At this point some simplifying notation will be used to reduce the cumbersome multiple subscripts, particularly, the eight subscripts on $\hat{\Gamma}$. Instead of the quadruple sum over ℓ, m, n, and k, a single running subscript will be used to identify these elements, e.g., A_{1111} will be A_1, $A_{1112} = A_2$, ... $A_{MMMK} = A_{(M \cdot M \cdot M \cdot K)}$. Thus

$$A_{mnk}(t) = A_i(t) \quad , \tag{55}$$

where

$$i = 3[(n-1) + 3(m-1) + 9(\ell-1)] + k \tag{56}$$

with these notations Equation 54 becomes simply

$$\hat{\Phi}(\vec{r}_1, \vec{r}_2, E_1, E_2, w) = \sum_{i}^{\alpha} \sum_{j}^{\alpha} \hat{\Gamma}_{ij}(w) \psi_i(\vec{r}_1, E_1) \psi_j(\vec{r}_2, E_2) \tag{57}$$

where

$$\alpha = (M \cdot M \cdot M \cdot K) \quad .$$

The key to finding the time coefficients is to note that for most modal analysis methods the time coefficients are given by a set of differential equations of the form

$$[D][A] = [f] \tag{58}$$

where [D] is a matrix whose elements are constants and

linear differential operators, [A] is a vector containing the time coefficients and [f] is a vector of driving functions.

The required expressions for the Γ_{ij} can be developed from the following general problem. Consider the system

$$\begin{aligned}
&D_{11}A_1(t) + D_{12}A_2(t) + \ldots + D_{1\alpha}A_\alpha(t) = f_1(t) \\
&D_{21}A_1(t) + \ldots \qquad\qquad + D_{2\alpha}A_\alpha(t) = f_2(t) \\
&\quad\vdots \qquad\qquad\qquad\qquad\qquad\quad \vdots \\
&D_{\alpha 1}A_1(t) + D_{\alpha 2}A_2(t) + \ldots + D_{\alpha\alpha}A_\alpha(t) = f_\alpha(t)
\end{aligned} \tag{59}$$

It is assumed that $A_j(t)$ and $f_i(t)$ are time stationary ergodic random functions. At this point introduce the output correlation function

$$\begin{aligned}
\Gamma_{ij}(\tau) &= \overline{A_i(t)A_j(t+\tau)} \\
&= \lim_{T\to\infty} \frac{1}{T} \int_{-T/2}^{T/2} A_i(t)A_j(t+\tau)dt \quad ,
\end{aligned} \tag{60}$$

and the input correlation function

$$\begin{aligned}
\chi_m(\tau) &= \overline{f_{\ }(t)f_m(t+\tau)} \\
&= \lim_{T\to\infty} \frac{1}{T} \int_{-T/2}^{T/2} f_{\ }(t)f_m(t+\tau)dt \quad .
\end{aligned} \tag{61}$$

$\Gamma_{ij}(\tau)$ can be thought of as an element in a general output correlation matrix $[\Gamma(\tau)]$, and χ_m as an element of a general input correlation matrix $[\chi(\tau)]$. There are related spectral density matrices $[\hat{\Gamma}(w)]$ and $[\hat{\chi}(w)]$.

To develop the desired relationship, operate on Equation 60 with $\bar{D}_{Pj}$ which is the same as D_{Pj} except differentiation is taken with respect to τ rather than t. (Note $\bar{D}_{Pj}$ is <u>not</u> a matrix.) The result is

$$\bar{D}_{Pj}\Gamma_{ij}(\tau) = \lim_{T\to\infty} \frac{1}{T} \int_{-T/2}^{T/2} A_i(t)\bar{D}_{Pj}A_j(t+\tau)dt \quad , \tag{62}$$

which upon summing over j becomes

$$\sum_{j=1}^{\alpha} \bar{D}_{Pj}\Gamma_{ij}(\tau) = \lim_{T\to\infty} \frac{1}{T} \int_{-T/2}^{T/2} A_i(t)\left[\sum_{j=1}^{\alpha} \bar{D}_{Pj}A_j(t+\tau)\right]dt \quad . \tag{63}$$

The derivatives with respect to τ in $\bar{D}_{Pj}$ can be replaced with derivatives with respect to $(t+\tau)$ in the sum on the R.H.S. of Equation 63. Thus, this sum is the same as the L.H.S. of the p^{th} equation in Equation 59 with t replaced with $t+\tau$. As a result

$$\sum_{j=1}^{\alpha} \bar{D}_{pj}A_j(t+\tau) = f_p(t+\tau) \quad , \tag{64}$$

and Equation 63 can be written as

$$\sum_{j=1}^{\alpha} \bar{D}_{Pj}\Gamma_{ij}(\tau) = \lim_{T\to\infty} \frac{1}{T} \int_{-T/2}^{T/2} A_i(t) f_p(t+\tau)\,dt \quad . \qquad (65)$$

On the R.H.S. of Equation 65, let $\gamma = t+\tau$, yielding

$$\sum_{j=1}^{\alpha} \bar{D}_{Pj}\Gamma_{ij}(\tau) = \lim_{T\to\infty} \frac{1}{T} \int_{-T/2}^{T/2} A_i(\gamma-\tau) f_p(\gamma)\,d\gamma \quad , \qquad (66)$$

but since γ is a dummy variable of integration one can replace γ with t to obtain

$$\sum_{j=1}^{\alpha} \bar{D}_{Pj}\Gamma_{ij}(\tau) = \lim_{T\to\infty} \frac{1}{T} \int_{-T/2}^{T/2} A_i(t-\tau) f_p(t)\,dt \quad . \qquad (67)$$

Next introduce the operators $\bar{D}^{-}_{qi}$ which operate on τ and have the signs changed on all derivatives of odd power. Operation on Equation 67 with $\bar{D}^{-}_{qi}$ yields

$$\sum_{j=1}^{\alpha} \bar{D}^{-}_{qi}\bar{D}_{Pi}\Gamma_{ij}(\tau) = \lim_{T\to\infty} \frac{1}{T} \int_{-T/2}^{T/2} f_p(t)\bar{D}^{-}_{qi}A_i(t-\tau)\,dt \quad . (68)$$

Summing on the i index gives

$$\sum_{i=1}^{\alpha}\sum_{j=1} \bar{D}^{-}_{qi}D_{Pi}\Gamma_{ij}(\tau) = \lim_{T\to\infty} \frac{1}{T} \int_{-T/2}^{T/2} f_p(t)\Big[\sum_{i=1}^{a} \bar{D}^{-}_{qi}A_i(t-\tau)\Big]dt \quad . \qquad (69)$$

Note that derivatives with respect to $(t-\tau)$ of a function such as A_i in Equation 69 equal the derivatives with respect

to τ except for a sign change on derivatives of odd power. Thus, one can see that the sum on the R.H.S. of Equation 69 is the same as the L.H.S. of the q^{th} equation in Equations 59 with t replaced by $(t-\tau)$. Hence

$$\sum_{i=1}^{\alpha} \bar{D}^{-}_{qi} A_i(t-\tau) = f_q(t-\tau) \quad , \tag{70}$$

and

$$\sum_{i=1}^{\alpha}\sum_{j=1}^{\alpha} \bar{D}^{-}_{qi}\bar{D}_{Pi}\Gamma_{ij}(\tau) = \lim_{T\to\infty}\frac{1}{T}\int_{-T/2}^{T/2} f_p(t)f_q(t-\tau)dt \quad . \tag{71}$$

By making a change in the variable of the R.H.S., $\mu = t-\tau$, Equation 71 becomes

$$\sum_{i=1}^{\alpha}\sum_{j=1}^{\alpha} \bar{D}^{-}_{qi}\bar{D}_{Pi}\Gamma_{ij}(\tau) = \lim_{T\to\infty}\frac{1}{T}\int_{-T/2}^{T/2} f_q(\mu)f_p(\mu+\tau)d\mu \quad . \tag{72}$$

Noting that μ is merely a dummy variable of integration, it follows that

$$\sum_{i=1}^{\alpha}\sum_{j=1}^{\alpha} \bar{D}^{-}_{qi}\bar{D}_{Pi}\Gamma_{ij}(\tau) = \chi_{qp}(\tau) \quad . \tag{73}$$

Equation 73 represents a system of α^2 linear differential equations in the $\Gamma_{ij}(\tau)$. This can be changed to a set of algebraic equations by Fourier transforming both sides, yielding

$$\sum_{i=1}^{\alpha}\sum_{j=1}^{\alpha} \hat{\bar{D}}^{-}_{qi}\hat{\bar{D}}_{Pi}\hat{\Gamma}_{ij}(w) = \hat{\chi}_{qP}(w) \quad . \tag{74}$$

$\hat{\bar{D}}_{Pi}$ is obtained from $\bar{D}_{Pi}$ by replacing $\frac{d}{d}$ with jw, where j is the so-called "imaginary unit", i.e., $j^2 = -1$. $\hat{\bar{D}}^{-}_{qi}$ is obtained from $\bar{D}^{-}_{qi}$ by replacing $\frac{d}{d}$ by jw. Thus $\hat{\bar{D}}_{Pi}$ is the Fourier transform of the original operator D_{Pi} and, due to the sign changes in $\bar{D}^{-}_{qi}$, $\hat{\bar{D}}^{-}_{qi}$ is the complex conjugate of the Fourier transformed original operator D_{qi}.

Equation 74 can be written in matrix form and solved for the $\hat{\Gamma}$ matrix. Written in matrix form Equation 74 is

$$[\hat{D}]^{*}[\hat{\Gamma}][\hat{D}]^{T} = [\hat{\chi}] \quad . \tag{75}$$

Solving this for $[\hat{\Gamma}]$ yields

$$[\hat{\Gamma}] = [\hat{D}^{*}]^{-1}[\hat{\chi}][\hat{D}^{T}]^{-1} \quad , \tag{76}$$

where

$[\hat{D}]$ = Fourier transform of original D matrix, [D]

$[\hat{D}^{*}]$ = Complex conjugate of $[\hat{D}]$.

Using the notation introduced in Equation 55, i.e., $A_{mnk} = A_i$, the eigenvalue problem of Equation 15 becomes

$$L_o\vec{\psi}_i(\vec{r}) = \lambda_i\vec{\psi}_i(\vec{r}) \quad . \tag{77}$$

Similarly, the equations for the time coefficients may then be written as

$$\begin{aligned}
\frac{dA_1}{dt} - \lambda_1 A_1 &= \langle \vec{\psi}_1^{+}, L_1 \Phi_o \rangle / \langle \vec{\psi}_1^{+}, \vec{\psi}_1 \rangle \\
\frac{dA_2}{dt} - \lambda_2 A_2 &= \langle \vec{\psi}_2^{+}, L_1 \Phi_o \rangle / \langle \vec{\psi}_1^{+}, \vec{\psi}_1 \rangle \\
&\vdots \\
\frac{dA_\alpha}{dt} - \lambda_\alpha A_\alpha &= \langle \vec{\psi}_\alpha^{+}, L_1 \Phi_o \rangle / \langle \vec{\psi}_\alpha^{+}, \vec{\psi}_\alpha \rangle \quad .
\end{aligned} \tag{78}$$

Or in matrix form this is

$$\begin{bmatrix}
\frac{d}{dt} - \lambda_1 & & & \\
& \frac{d}{dt} - \lambda_2 & & \\
& & \ddots & \\
& & & \frac{d}{dt} - \lambda_\alpha
\end{bmatrix}
\begin{bmatrix} A_1 \\ A_2 \\ \vdots \\ A_\alpha \end{bmatrix}
=
\begin{bmatrix}
\langle \vec{\psi}_1^{+}, L_1 \Phi_o \rangle / \langle \vec{\psi}_1^{+}, \vec{\psi}_1 \rangle \\
\\
\\
\langle \vec{\psi}_\alpha^{+}, L_1 \Phi_o \rangle / \langle \vec{\psi}_\alpha^{+}, \vec{\psi}_\alpha \rangle
\end{bmatrix} \quad . \tag{79}$$

Comparison of Equation 79 with Equations 58 and 59 reveals that the driving functions, f_i, for the Natural Mode Approximation are given by

$$f_i = \frac{\langle \vec{\psi}_1^{+}, L_1 \Phi_o \rangle}{\langle \vec{\psi}_i^{+}, \vec{\psi}_i \rangle} \quad . \tag{80}$$

Let n_i and d_i represent the numerator and denominator of $f_i(t)$ respectively. Thus,

$$f_i(t) = \frac{n_i(t)}{d_i} \tag{81}$$

where

$$n_i(t) = \langle \vec{\psi}_i^{+}, L_1 \Phi_o \rangle \tag{81a}$$

$$d_i = \langle \vec{\psi}_i^{+}, \vec{\psi}_i \rangle \quad . \tag{81b}$$

Consider a perturbation of the group 2 absorption cross section about its steady-state value. For a one-dimensional case with the perturbation occurring between the space points $x = a_1$ and $x = a_2$

$$\Delta\Sigma_{a2}(x,t) = \begin{cases} \delta\Sigma_a P(t) & a_1 \leq x \leq a_2 \\ 0 & x < a_1,\ x > a_2 \end{cases} , \tag{82}$$

where $P(t)$ is the time dependence of the perturbation. Thus, for a two energy group, one delayed group formulation, $n_i(t)$ is found to be

$$n_i(t) = \int_{\text{reactor}} [(\psi_i^{+})_1 \ (\psi_i^{+})_2 \ (\psi_i^{+})_3] \begin{bmatrix} 0 & 0 & 0 \\ 0 & V_2\Delta\Sigma_{a2} & 0 \\ 0 & 0 & 0 \end{bmatrix} \begin{bmatrix} \phi_o^1 \\ \phi_o^2 \\ C_o \end{bmatrix} dx$$

$$= \int_{\text{reactor}} (\psi_i^{+}(x))_2 V_2 \Delta\Sigma_{a2}(x,t) \phi_o^2(x) dx$$

$$= P(t) V_2 \delta\Sigma_a \int_{a_i}^{a_2} [\psi_i^+(x)]_2 \, \phi_o^2(x) dx$$

$$= P(t) I_i \quad , \tag{83}$$

where

$$I_i = V_2 \delta\Sigma_a \int_{a_i}^{a_2} (\psi_i(x))_2 \, \phi_o^2(x) dx \quad . \tag{84}$$

Similarly, d_i is found to be

$$d_i = \int_{\text{reactor}} [(\psi_i^+)_1 \; (\psi_i^+)_2 \; (\psi_i^+)_3] \begin{bmatrix} \psi_i^1 \\ \psi_i^2 \\ \psi_i^3 \end{bmatrix} dx \quad . \tag{85}$$

As a result,

$$f_i(t) = \frac{I_i}{d_i} P(t)$$

$$= K_i P(t) \quad . \tag{86}$$

Forming the auto-correlation function of $f_i(t)$ yields

$$\phi_{f_\ell f_m}(\tau) = \overline{f_\ell(t) f_m(t+\tau)}$$

$$= K_\ell K_m \, \overline{P(t) P(t+\tau)} \quad . \tag{87}$$

If Equation 87 is Fourier transformed

$$\Phi_{f_\ell f_m}(w) = K_\ell K_m \Phi_{PP}(w) \quad , \tag{88}$$

where $\Phi_{PP}(w)$ is the spectral density of the time variation of $\Delta\Sigma_a$.

It can be seen that the $\phi_{f_\ell f_m}(\tau)$ of Equation 87 is the $\chi_{\ell m}(\bar{\tau})$ of Equation 61, i.e.,

$$\chi_{\ell m}(\bar{\tau}) = K_\ell K_m \overline{P(t)P(t+\bar{\tau})}$$

$$= C_{\ell m}\phi_{PP}(\bar{\tau}) \quad , \tag{89}$$

and further

$$\hat{\chi}_{\ell m}(w) = C_{\ell m}\Phi_{PP}(w) \quad . \tag{90}$$

In matrix form Equations 89 and 90 become

$$[\chi(\bar{\tau})] = \phi_{PP}(\bar{\tau})[C] \tag{91}$$

and

$$[\hat{\chi}(w)] = \Phi_{PP}(w)[C] \tag{92}$$

respectively, where ϕ_{PP} and Φ_{PP} are scalers.

Thus if $\Phi_{PP}(w)$ is known, one can calculate $\hat{\chi}_{\ell m}(w)$, and knowing $[\hat{\chi}]$ and $[\hat{D}]$ one can calculate $[\hat{\Gamma}]$ by Equation 76. Then once $[\hat{\Gamma}]$ is known, Equation 57 will yield the spectral density function of the flux. The Fourier inverse of the spectral density will then yield the flux auto-correlation

function.

At this point, an important observation is made. Note that the time dependent function P(t) is the same for all modes, obviously $\Phi_{pp}(w)$ is likewise. The various $f_i(t)$ differ only by multiplicative constants. As a result, once $\Phi_{pp}(w)$ is determined, it can be used to calculate the effect of perturbations, having this time dependence, located at any point in the reactor.

V. MATHEMATICAL MODELS AND ANALYSIS

A. Reactor Model

The reactor model for this investigation is a bare homogeneous parallelpiped (see Figure 2). The reactor parameters are characteristic of the current fast sodium-cooled 1000 Mwe Design Studies. In particular, the volume fractions are: 52% sodium, 30% fuel, and 18% stainless steel.

The two energy group one delayed neutron group diffusion theory equations used to describe the reactor dynamics are:

$$D_1\nabla^2\phi_1 - \Sigma^{1\to2}\phi_1 - \Sigma_{a1}\phi_1 + \nu_2\Sigma_{f2}\phi_2(1-\beta)\chi_1 + \nu_1\Sigma_{f1}\phi_1(1-\beta)\chi_1 = \frac{1}{V_1}\frac{\partial\phi_1}{\partial t} \tag{93}$$

$$D_2\nabla^2\phi_2 - \Sigma_{a2}\phi_2 + \Sigma^{1\to2}\phi_1 + \nu_2\Sigma_{f2}\phi_2(1-\beta)\chi_2 + \nu_1\Sigma_{f1}\phi_1(1-\beta)\chi_2 + \lambda C = \frac{1}{V_2}\frac{\partial\phi_2}{\partial t} \tag{94}$$

$$\nu_1\Sigma_{f1}\phi_1\beta + \nu_2\Sigma_{f2}\phi_2\beta - \lambda C = \frac{\partial C}{\partial t} \quad . \tag{95}$$

In these equations it has been assumed that all delayed neutrons are born into group 2, and the homogenized group

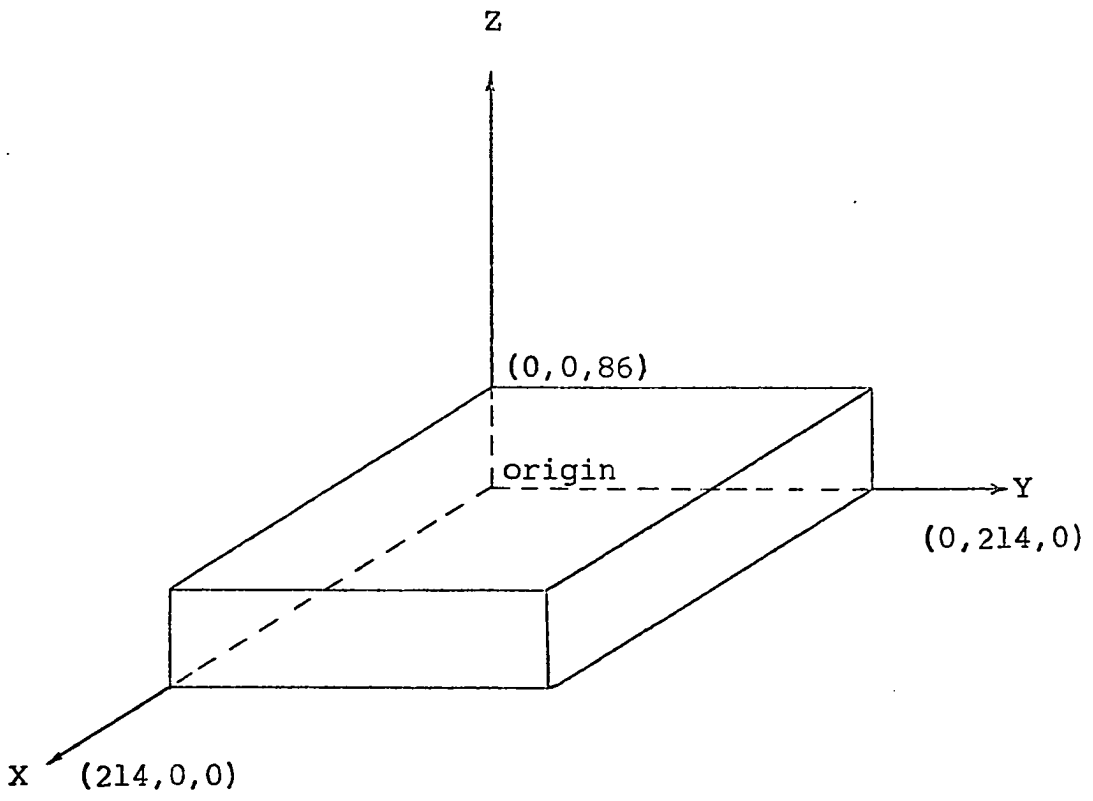

Figure 2. Geometry of reactor model

parameters are defined as:

ϕ_i = group i neutron flux at space point (x,y,z)

D_i = diffusion coefficient for group i

$\Sigma^{1\to2}$ = macroscopic elastic plus inelastic scattering cross section for scattering from group 1 to group 2

Σ_{ai} = group i macroscopic absorption cross section

Σ_{fi} = group i macroscopic fission cross section

ν_i = average number of neutrons produced per fission occurring in group i

χ_i = fraction of fission spectrum falling into group i (assumed identical for all fissionable isotopes)

V_i = group i neutron velocity

β = effective delayed neutron fraction

λ = delayed neutron group decay constant

C = concentration of delayed neutron precursors

∇^2 = Laplacian operator .

The microscopic cross sections used in this investigation were obtained by collapsing a 16 Group Set of fast reactor cross sections (106) to two groups. The two energy groups were split at the U-238 Fission threshold of 1.35 MeV. Simple flux weighting was employed in collapsing the

cross sections (107,108). A flux energy spectrum representative of a carbide fueled fast sodium cooled reactor (109) was utilized in the collapsing process. Using representative volume fractions, temperatures, isotopic compositions, etc., found in the literature (1, 110, 111, 112) the macroscopic cross sections were then determined. Similarly, the other homogenized group parameters were calculated or found in the literature. For a more complete discussion on the method used to collapse the 16 group set of fast reactor constants to two groups, see Appendix A.

Under equilibrium conditions, Equations 93, 94 and 95 reduce to a set of two coupled second-order differential equations. That is, ϕ_2 appears in the equation for ϕ_1, and ϕ_1 appears in the equation for ϕ_2. In eliminating ϕ_2 from the equation for ϕ_1, a fourth-order differential equation evolves. This fourth order equation can then be solved by factoring (113). Following this standard procedure and taking the origin of the rectangular coordinate system to be at the lower left back corner of the reactor as shown in Figure 1, solutions for the group fluxes are found to be

$$\phi_1(x,y,z) = P \sin \frac{\pi}{a}x \sin \frac{\pi}{b}y \sin \frac{\pi}{c}z \qquad (96)$$

$$\phi_2(x,y,z) = PS \sin \frac{\pi}{a}x \sin \frac{\pi}{b}y \sin \frac{\pi}{c}z \quad . \qquad (97)$$

Here S is a "coupling coefficient" determined by the reactor

materials, and P is an arbitrary constant determined by the reactor power level. This procedure also yields an expression for the material buckling which can then be employed to determine the critical dimensions and/or material compositions. The steady state reactor parameters are given in Table 1.

Table 1. Steady state reactor parameters

Parameter	Units	Value
D_1	cm	3.2000
D_2	cm	2.0310
$\Sigma^{1\to2}$	cm^{-1}	0.0394480
Σ_{a1}	cm^{-1}	0.0006648
Σ_{a2}	cm^{-1}	0.0029600
Σ_{f1}	cm^{-1}	0.0066876
Σ_{f2}	cm^{-1}	0.0018335
ν_1	neutrons/fission	3.07880
ν_2	neutrons/fission	2.88350
χ_1	--	0.577
χ_2	--	0.423
v_1	cm/sec	2.6170×10^9
v_2	cm/sec	1.0380×10^9
β	--	0.00345
λ	sec^{-1}	0.0822493
a	cm	214.2455
H	cm	85.69821

B. Determining the Eigenvalues and Eigenvectors

From the equations modeling the reactor, i.e., Equations 93, 94, and 95, one can see that the steady state matrix operator is

$$[L_o]_M =$$

$$\begin{bmatrix} V_1[-D_1B_M^2-\Sigma^{1\to2}-\Sigma_a+\nu_1\Sigma_{f1}(1-\beta)\chi_1] & V_1\nu_2\Sigma_{f2}(1-\beta)\chi_1 & 0 \\ V_2[\Sigma^{1\to2}+\nu_1\Sigma_{f1}(1-\beta)\chi_2 & V_2[-D_2B_M^2-\Sigma_{a2}+\nu_2\Sigma_{f2}(1-\beta)\chi_2] & \tfrac{1}{2}\lambda \\ \nu_1\Sigma_{f1}\beta & \nu_2\Sigma_{f2}\beta & -\lambda \end{bmatrix}$$

(98)

The first step in employing the Natural Mode Approximation is the determination of the base vectors or spatial eigenvectors, $\vec{\psi}_{Mk}(x,y,z)$. The spatial function part, $S_M(x,y,z)$, is found as the normalized solution of

$$\nabla^2 S(x,y,z) + B_M^2\, S(x,y,z) = 0 \quad . \tag{99}$$

For the reactor model considered in this work

$$S_M(x,y,z) = S_{\ell,m,n}(x,y,z)$$

$$= \sin\frac{\ell\pi}{214.24}x \sin\frac{m\pi}{214.24}y \sin\frac{n\pi}{85.70}z \quad . \tag{100}$$

The real problem in determining $\vec{\psi}_{Mk}$ is then in finding the relative amplitude vector, $\vec{e}_{Mk}$. That is, the more difficult part of calculating the spatial eigenvectors is finding the eigenvalues and eigenvectors of the steady state matrix operator.

At first thought one might think this to be a relatively simple problem with today's computers and software. Actually there are two minor difficulties encountered in attempting to calculate the eigenvalues and eigenvectors. First, although there are sufficient subroutines for accomplishing this task for symmetric matrices, the standard Fortran library of subroutines (114) has available no routine to find the eigenvalues and eigenvectors of a general non-symmetric matrix. It is quickly found that the steady state matrix operator is indeed non-symmetric.

The second difficulty arises due to the elements of L_o being so vastly different in magnitude among themselves. The elements of L_o range from approximately 9×10^7 down to zero. The largest and smallest eigenvalue, for a given mode, also differ by a factor of approximately 10^9. For each mode there are two eigenvalues of large magnitude ($\tilde{}-2 \times 10^7$) and one of small ($\tilde{}-8 \times 10^{-2}$) magnitude. Obviously, this "ill condition" of the matrix creates problems when operations such as subtraction are involved in a routine to find the eigenvectors or eigenvalues.

These minor difficulties were overcome by using the subroutine HSBG in conjunction with ATEIG (114). HSBG reduces a real matrix into upper almost triangular or Hessenberg form. ATEIG computes the eigenvalues of a real almost triangular matrix. Thus these two programs enable one to find the eigenvalues of the steady state matrix operator.

For this work, 3 modes in each of the three dimensions will be considered. Thus the summations over ℓ, m, and n will be from 1 to 3. This results in 27 modes being considered with three eigenvalues per mode or 81 eigenvalues. The eigenvalues for each mode are presented in Table 2.

There were no subroutines available for finding the eigenvector corresponding to each eigenvalue. Thus a program found the eigenvectors as normalized solutions to the matrix equation

$$[R]\vec{e} = [0] \quad , \tag{101}$$

where the matrix [R] is given by

$$[R] = [L_o]_{\ell mn} - \lambda_{\ell mn}[I] \quad , \tag{102}$$

and $\vec{e}$ is the eigenvector to be found. Since the determinant of the coefficient matrix, R, is zero, a solution for $\vec{e}$ is then the co-factors along any row of the matrix R (115).

Table 2. Eigenvalues

Mode					Buckling	Eigenvalue
	m	n	k	i	$B^2_{mn} \times 10^2$	e_{mnk}
1	1	1	1	1	0.17739	0.0
1	1	1	2	2		-0.24344×10^{5}
1	1	1	3	3		-0.93322×10^{8}
1	1	2	1	4	0.58055	-0.82049×10^{-1}
1	1	2	2	5		-0.94848×10^{7}
1	1	2	3	6		-0.12612×10^{9}
1	1	3	1	7	1.25248	-0.82176×10^{-1}
1	1	3	2	8		-0.24588×10^{8}
1	1	3	3	9		-0.18145×10^{9}
1	2	1	1	10	0.24189	-0.80988×10^{-1}
1	2	1	2	11		-0.15704×10^{7}
1	2	1	3	12		-0.98537×10^{8}
1	2	2	1	13	0.64505	-0.82077×10^{-1}
1	2	2	2	14		-0.10962×10^{8}
1	2	2	3	15		-0.13140×10^{9}
1	2	3	1	16	1.31698	-0.82179×10^{-1}
1	2	3	2	17		-0.26012×10^{8}
1	2	3	3	18		-0.18679×10^{9}
1	3	1	1	19	0.34940	-0.81775×10^{-1}
1	3	1	2	20		-0.41162×10^{7}
1	3	1	3	21		-0.10726×10^{9}
1	3	2	1	22	0.7256	-0.82109×10^{-1}
1	3	2	2	23		-0.13409×10^{8}
1	3	2	3	24		-0.14022×10^{9}
1	3	3	1	25	1.42449	-0.82186×10^{-1}
1	3	3	2	26		-0.28379×10^{8}
1	3	3	3	27		-0.19569×10^{9}

Table 2 (Continued)

Mode					Buckling	Eigenvalue
	m	n	k	i	$B^2_{mn} \times 10^2$	e_{mnk}
2	1	1	1	28	0.24189	-0.80988×10^{-1}
2	1	1	2	29		-0.15703×10^{7}
2	1	1	3	30		-0.98537×10^{8}
2	1	2	1	31	0.64505	-0.82077×10^{-1}
2	1	2	2	32		-0.10962×10^{8}
2	1	2	3	33		-0.13140×10^{9}
2	1	3	1	34	1.31698	-0.82179×10^{-1}
2	1	3	2	35		-0.26012×10^{8}
2	1	3	3	36		-0.18679×10^{9}
2	2	1	1	37	0.30640	-0.81616×10^{-1}
2	2	1	2	38		-0.31021×10^{7}
2	2	1	3	39		-0.10376×10^{9}
2	2	2	1	40	0.70955	-0.82098×10^{-1}
2	2	2	2	41		-0.12432×10^{8}
2	2	2	3	42		-0.13669×10^{9}
2	2	3	1	43	1.38149	-0.82183×10^{-1}
2	2	3	2	44		-0.27433×10^{8}
2	2	3	3	45		-0.19213×10^{9}
2	3	1	1	46	0.41391	-0.81905×10^{-1}
2	3	1	2	47		-0.56274×10^{7}
2	3	1	3	48		-0.11251×10^{9}
2	3	2	1	49	0.81706	-0.82124×10^{-1}
2	3	2	2	50		-0.14868×10^{8}
2	3	2	3	51		-0.14553×10^{9}
2	3	3	1	52	1.48900	-0.82189×10^{-1}
2	3	3	2	53		-0.29796×10^{8}
2	3	3	3	54		-0.20103×10^{9}

Table 2 (Continued)

Mode					Buckling	Eigenvalue
	m	n	k	i	$B^2_{mn} \times 10^2$	e_{mnk}
3	1	1	1	55	0.34940	-0.81775×10^{-1}
3	1	1	2	56		-0.41162×10^{7}
3	1	1	3	57		-0.10726×10^{9}
3	1	2	1	58	0.75256	-0.82109×10^{-1}
3	1	2	2	59		-0.13409×10^{8}
3	1	2	3	60		-0.14022×10^{9}
3	1	3	1	61	1.42449	-0.82186×10^{-1}
3	1	3	2	62		-0.28379×10^{8}
3	1	3	3	63		-0.19569×10^{9}
3	2	1	1	64	0.41391	-0.81905×10^{-1}
3	2	1	2	65		-0.56274×10^{7}
3	2	1	3	66		-0.11251×10^{9}
3	2	2	1	67	0.81706	-0.82124×10^{-1}
3	2	2	2	68		-0.14868×10^{8}
3	2	2	3	69		-0.14553×10^{9}
3	2	3	1	70	1.48900	-0.82189×10^{-1}
3	2	3	2	71		-0.29796×10^{8}
3	2	3	3	72		-0.20103×10^{9}
3	3	1	1	73	0.52141	-0.82013×10^{-1}
3	3	1	2	74		-0.81231×10^{7}
3	3	1	3	75		-0.12128×10^{9}
3	3	2	1	76	0.92457	-0.82142×10^{-1}
3	3	2	2	77		-0.17287×10^{8}
3	3	2	3	78		-0.15438×10^{9}
3	3	3	1	79	1.5965	-0.82193×10^{-1}
3	3	3	2	80		-0.32152×10^{8}
3	3	3	3	81		-0.20995×10^{9}

C. Noise Analysis of Reactor Model

This investigation considers two sources of neutron flux noise. First, there is the random driving function due statistical variations in the number of neutrons produced per fission, and in the neutron leakage and absorption processes. It will be assumed that this is represented approximately by a "white" noise spectrum as first suggested by Moore (81). White noise refers to noise with a spectral density which is constant, i.e., noise which is composed of equal contributions from all frequencies. Second, neutron flux perturbations will be excited by simulating the occurrence of localized sodium boiling.

The "white" noise will manifest itself in the elements of the first two columns of the operator matrix, L. The boiling noise is assumed to effect the transfer cross section $\Sigma^{1\to2}$, absorbtion cross sections, and neutron leakage. The occurrence of sodium boiling then shows up as perturbations in elements L_{11}, L_{21}, and L_{22}.

The neutron yield per fission may be represented as $\nu = \nu_o + \delta\nu(t)$, where ν_o is the average yield and $\delta\nu(t)$ is the time dependent random variation which has a time-average value of zero. The other driving functions can likewise be so represented. As a result, the perturbation matrix, L_1, can be written as

$$L_1(t) = \begin{bmatrix} V_1(\delta F_{11} + \delta B_{11}) & V_1 \delta F & 0 \\ V_2(\delta F_{12} + \delta B_{12}) & V_2(\delta F_{22} + \delta B_{22}) & 0 \\ \delta F_{31} & \delta F_{32} & 0 \end{bmatrix} , \quad (103)$$

where δF represents the white driving function and δB represents the boiling induced driving function.

This investigation considers the boiling perturbation to be represented by

$$\delta B_{ij}(t,\vec{r}) = \begin{cases} M_{ij} P(t)[1 - \exp(-\gamma \ell)] , & X_L \le x \le X_U \\ & Y_L \le y \le Y_U \\ & Z_L \le z \le Z_U \\ 0 \quad \text{all other } x,y,z \end{cases} \quad (104)$$

where

$\ell \equiv Z - Z_L$

$M \equiv$ amplitude of variation

$P(t) \equiv$ time dependence of variation

$\gamma \equiv$ boiling parameter.

Thus it is seen that the boiling begins at an elevation of $Z = Z_L$, and the "boiling parameter" determines how fast the boiling increases along the coolant channel until it reaches its maximum perturbation value, M. The boiling occurs only within the boundaries prescribed by X_L, X_U, Y_L, Y_U, Z_L and Z_U.

The white noise will be denoted by

$$\delta F_{ij}(t) = NW(t) \quad , \tag{105}$$

where N is the amplitude of variation and W(t) is the time dependence of this variation. Note that δF is not a function of space since fission etc. occurs at every point in the reactor.

The expression for $n_i(t)$ given in Equation 81a will now be somewhat more complicated than the simple illustrative case considered previously, where the perturbation was given by Equation 82. Using the above notations, $n_i(t)$ is given as

$$n_i(t) =$$

$$\int_{\text{reactor}} [\psi_i^{+1}\psi_i^{+2}\psi_i^{+3}] \begin{bmatrix} V_1(\delta F_{11}+\delta B_{11}) & V_1\delta F_{12} & 0 \\ V_2(\delta F_{21}+\delta B_{21}) & V_2(\delta F_{22}+\delta B_{22}) & 0 \\ \delta F_{31}+\delta B_{31} & \delta F_{32} & 0 \end{bmatrix} \begin{bmatrix} \phi_o^1 \\ \phi_o^2 \\ C_o \end{bmatrix} dxdydz$$

$$= \int_{\text{reactor}} [\delta F_{11}V_1\psi_i^{+1}\phi_o^1 + \delta F_{12}V_1\psi_i^{+1}\phi_o^2 + \delta F_{21}V_2\psi_i^{+2}\phi_o^1 + \delta F_{22}V_2\psi_i^{+2}\phi_o^2$$

$$+ \delta F_{31}\psi_i^{+3}\phi_o^1 + \delta F_{32}\psi_i^{+3}\phi_o^2 + \delta B_{11}V_1\psi_i^{+1}\phi_o^1$$

$$+ \psi_i^{+2}V_2(B_{21}\phi_o^1 + B_{22}\phi_o^2)]dxdydz \quad . \tag{106}$$

This $n_i(t)$ is equal to the sum of nine integrals. Six of these, corresponding to the white noise, are integrals over

the entire reactor. The remaining three, resulting from localized boiling, are integrals only over the volume of the perturbation since the perturbation is zero except for $X_L \leq X \leq X_U$, $Y_L \leq Y \leq Y_U$, and $Z_L \leq Z \leq Z_U$. Denoting these integrals by I_1, I_2, ... I_q, then $n_i(t)$ can be written simply as

$$n_i(t) = (I_1 + I_2 + \ldots + I_9)_i \quad . \tag{107}$$

As shown in Appendix B, the first six integrals can be expressed as the product of a mode dependent factor and their time dependence,

$$(I_1 + I_2 + \ldots + I_6)_i = \eta_i W(t) \quad . \tag{108}$$

Furthermore, the interesting observation that $\eta_i = 0$ when $i \geq 4$ is shown in the Appendix. Similarly, it is shown in Appendix B that the last three integrals can be represented as

$$(I_7 + I_8 + I_9)_i = \varepsilon_i W(t) \quad . \tag{109}$$

Now $n_i(t)$ can be written simply as

$$n_i(t) = \varepsilon_i P(t) + \eta_i W(t) \quad , \tag{110}$$

and the expression for the driving functions, f_i, given by Equation 81 becomes

$$f_i(t) = \frac{\varepsilon_i}{d_i}P(t) + \frac{\eta_i}{d_i}W(t)$$

$$= K_i P(t) + Q_i W(t) \quad . \tag{111}$$

Forming the auto-correlation function of $f_i(t)$ yields

$$\phi_{f_\ell f_m}(\tau) = \overline{f_\ell(t) f_m(t+\tau)}$$

$$= \overline{[K_\ell P(t) + Q_\ell W(t)][K_m P(t+\tau) + Q_m W(t+\tau)]}$$

$$= \overline{K_\ell K_m P(t)P(t+\tau)} + \overline{K_\ell Q_m P(t)W(t+\tau)}$$

$$+ \overline{Q_\ell K_m W(t)P(t+\tau)} + \overline{Q_\ell Q_m W(t)W(t+\tau)}$$

$$= K_\ell K_m \overline{P(t)P(t+\tau)} + Q_\ell Q_m \overline{W(t)W(t+\tau)} \quad , \tag{112}$$

where the fact that P(t) and W(t) are uncorrelated has been utilized. Fourier transforming Equation 112 yields

$$\Phi_{f_\ell f_m}(w) = K_\ell K_m \Phi_{PP}(w) + Q_\ell Q_m \Phi_{WW}(w) \quad , \tag{113}$$

where $\Phi_{PP}(w)$ and $\Phi_{WW}(w)$ are the spectral densities of the time variations of the boiling and white noise driving functions respectively.

Since $\phi_{f_\ell f_m}$, given by Equation 112, is identically the $\chi_{\ell m}(\bar{\tau})$ of Equation 61, the following expression results

$$\hat{\chi}_{\ell m}(w) = C_{\ell m}\Phi_{PP}(w) + R_{\ell m}\Phi(w) \quad . \tag{114}$$

This then is the expression which is employed in this investigation to find $[\hat{\Gamma}]$ by means of Equation 76. The $\hat{\Gamma}$ matrix is then utilized in Equation 57 to find the spectral density functions of the flux.

D. Feedback Model

When the neutron, or power, level in a nuclear reactor increases, there is a corresponding increase in the temperature of materials in the core. This temperature change is accompanied by a change in the effective multiplication factor, k, due to cross section and density changes. The relationship between the temperature and the change in k is generally expressed in terms of a temperature coefficient, α_T, with units $\delta k/^{o}F$. Thus, the coupling can be expressed by

$$\delta k(t) = \alpha_T \delta T(t) \quad . \tag{115}$$

In order to obtain a qualitative indication of the effect of temperature feedback on the reactor behavior, a simple feedback model is employed. Space independent reactor kinetics equations will be utilized in conjunction with temperature feedback via the Doppler temperature coefficient.

It is well known from reactor control theory that a good approximation for the no-feedback reactor transfer function, G(S) is given by (93)

$$\frac{\Delta N(S)}{\Delta K(S)} = G(S)$$

$$= \frac{n(o)}{\ell} \frac{S + \bar{\lambda}}{S(S+\beta/\ell)} \quad , \tag{116}$$

where

$\Delta N(S)$ = Laplace transform of $\delta n(t)$

$\Delta K(S)$ = Laplace transform of $\delta k(t)$

$n(o)$ = steady state neutron density level

ℓ = neutron lifetime

$\bar{\lambda}$ = average precursor decay constant

β = total delayed neutron fraction.

In block diagram notation, Equation 116 can be represented by

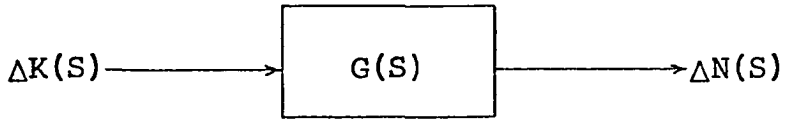

When feedback is taken into consideration, the reactor behavior can be represented by

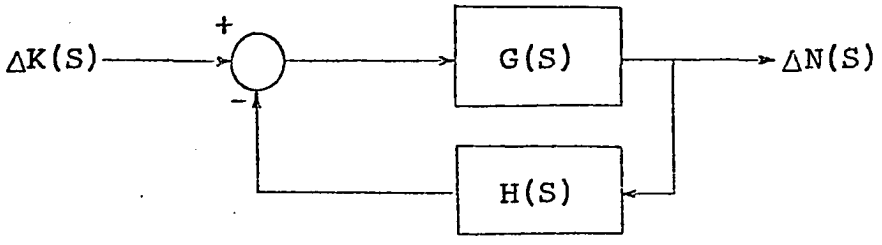

where H(S) is the feedback transfer function defined by

$$H(S) = \frac{\Delta K(S)}{\Delta N(S)} \quad . \tag{117}$$

To determine H(S), it is necessary to utilize relationships between the neutron level and the temperature of the fuel. These equations are obtained by writing heat balance equations for the fuel and for the sodium coolant. The fuel energy balance equation is

$$An(t) - H[T_f(t) - T_C(t)] = C_{Pf}M_f \frac{dT_f(t)}{dt} \quad , \tag{118}$$

where

A = factor relating neutron density to power production

H = heat transfer coefficient for heat transfer between fuel and coolant

T_f = average fuel temperature

T_C = average coolant temperature

C_{Pf} = specific heat of fuel

M_f = mass of fuel.

An energy balance applied to the sodium coolant yields

$$H[T_f(t) - T_C(t)] + T_i C_{PC} W - T_o(t) C_{PC} W = C_{PC} M_C \frac{d(T_o(t) + T_i)/2}{dt} \quad , \tag{119}$$

where

T_C = average coolant temperature

T_i = coolant inlet temperature (assumed constant)

T_o = coolant outlet temperature

W = coolant mass flow rate

M_C = mass of coolant in core

C_{PC} = specific heat of coolant.

These equations may be put in a simpler form by making use of the equilibrium relationships corresponding to t = 0 in Equations 118 and 119. By making the substitutions $n(t) = n(o) + \delta n(t)$, $T_o(t) = T_i + \Delta T(o) + \delta T(t)$, and $T_f(t) = T_f(o) + \delta T_f(t)$, these two equations will be in a form suitable for Laplace transforming. Upon Laplace transforming these equations and Equation 115, one will have three equations which may be solved simultaneously for $\Delta K(S)/\Delta N(S)$. The result is the feedback transfer function given by

$$H(S) = \frac{\alpha_T A(\tau_1 S + 1)/\tau_2\tau_1 H}{S^2+(\frac{\tau_1+\tau_2}{\tau_1\tau_2})S+\frac{D-1}{D\tau_1\tau_2}}, \qquad (120)$$

where

$\tau_1 = C_{PC}M_C/(2C_{PC}W + H)$

$\tau_2 = C_{Pf}M_f/H$

$$D = (2\ C_{PC}W + H)/H.$$

The parameters used in this investigation are given in Table 3.

Table 3. Parameters used in feedback model

Parameter	Units	Value
ℓ	seconds	1.418×10^{-7}
$\bar{\lambda}$	---	8.225×10^{-2}
β	---	3.45×10^{-3}
A	$(Btu/sec)/(_{o}n'/cm^3)$	2.72×10^{5}
H	$Btu/sec\,^{o}F$	2.21×10^{9}
T_f	^{o}F	1.800×10^{3}
T_C	^{o}F	1.000×10^{3}
C_{Pf}	$Btu/lb_m\,^{o}F$	0.062
M_f	lb_m	2.864×10^{3}
C_{PC}	$Btu/lb_m\,^{o}F$	0.300
T_i	^{o}F	850
T_o	^{o}F	1120
W	lb_m/sec	2.78×10^{4}
M_C	lb_m	2.72×10^{3}

VI. RESULTS AND CONCLUSIONS

The results presented here are the products of digital computer calculations based on Equation 54, which is reproduced here for convenient reference,

$$\hat{\Phi}(\vec{r}_1,\vec{r}_2,E_1,E_2) = \sum_{i=1}^{81}\sum_{j=1}^{81} \hat{\Gamma}_{ij}(w)\psi_i(\vec{r}_1,E_1)\psi_j(\vec{r}_2,E_2) \quad . \tag{121}$$

In this equation

$\hat{\Phi}$ = auto- or cross-spectral density function

$\vec{r}_1$ = location of detector no. 1

$\vec{r}_2$ = location of detector no. 2

E_1 = flux energy group measured at $\vec{r}_1$

E_2 = flux energy group measured at $\vec{r}_2$

w = frequency

$\hat{\Gamma}_{ij}$ = element of matrix defined in Equation 76; dependent on the spectral density of the input driving function.

If $E_1 = E_2$ and $\vec{r}_1 = \vec{r}_2$, then the resulting $\hat{\Phi}$ represents the neutron flux spectral density. When $\vec{r}_1 \neq \vec{r}_2$, Φ is equal to the neutron flux spatial cross spectral density. Also, if $E_1 \neq E_2$, then the result is the neutron flux energy cross-spectral density. If $\vec{r}_1 \neq \vec{r}_2$ and $E_1 \neq E_2$, the result of Equation 121 will be called the neutron flux spatial-and-

energy cross spectral density.

The spatial location of the boiling manifests itself in the calculations through the integrations involved in calculating the inner products of Equation 80. (This dependence is illustrated in Appendix B.)

For the results presented here, the detector locations may be identified by their coordinates based on the system shown in Figure 2,

$$\vec{r}_1 \rightarrow \text{pt.}(100,100,85)$$

and

$$\vec{r}_2 \rightarrow \text{pt.}(100,170,85) \quad .$$

To demonstrate that the mathematical model represents the system as intended, the neutron flux spectral density function was calculated utilizing a white boiling noise perturbation as the input driving function. The results of this calculation are shown in Figure 3. The spectral density function exhibits the shape characteristic of reactor transfer functions. The "straight line approximation" break frequencies are indicated on the plot as being 0.082 and 24,000 radians per second. From space-independent reactor kinetics it is known that the first break frequency occurs at a value of $\bar{\lambda}$, and the second break occurs at a frequency of β/ℓ radians per second. Thus the break fre-

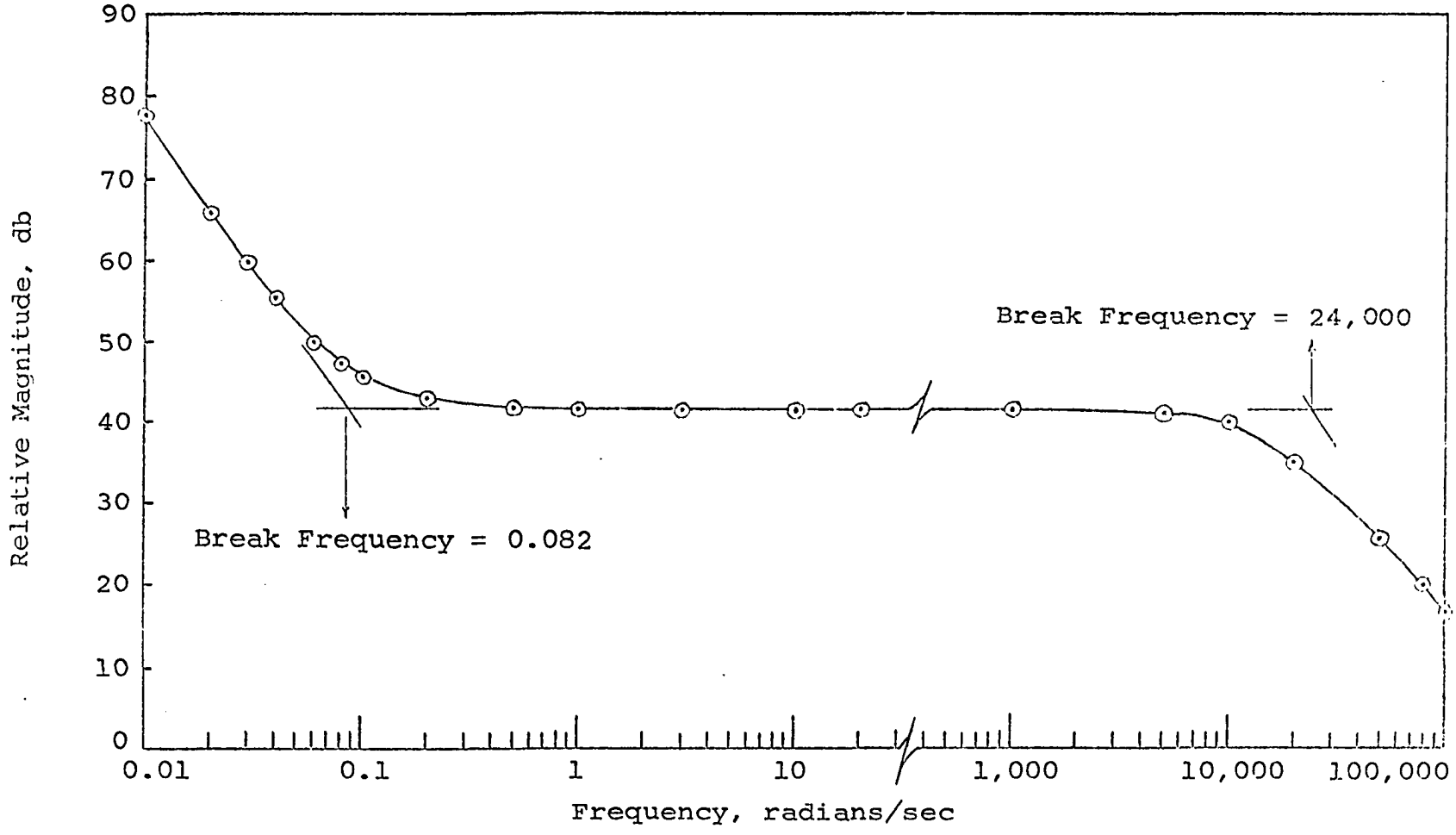

Figure 3. Neutron flux spectral density for white boiling input

quency of 0.082 compares very well with the value of $\bar{\lambda}$, which is for this mode, 0.08225.

Similarly, the value of the second break frequency, 24,000, compares very well with 24,322; the value of β/ℓ for this model. These values are characteristic of fast reactor systems. Table 4 compares the values of β/ℓ for several fast reactors with the value found in the present model. As can be seen from this table, the parameters of the model appear to be representative of fast reactor systems. Consequently, the reactor model and the noise formulation seem to be representing the system quite satisfactorily.

Table 4. Comparison of β/ℓ for various fast reactors

Reactor	β/ℓ [a]
EBR-II	90,000
Fermi	39,000
Rapsodie	65,000
A.I. design	6,600
C.E. design	16,200
Model	24,344

[a]Calculated from data given by Eggen (110); except for model.

Figure 4 shows the results of the calculation of the neutron flux spectral density based on a white fission noise perturbation. It also possesses the characteristics of the normal reactor transfer function. Upon closer examination however, there is a slight difference apparent in the behavior at low frequencies. The high frequency response is essentially identical for both cases.

This difference in the low frequency behavior shows up in a difference in break frequencies. In the case of boiling noise the break occurs at 0.082, whereas the break is at 0.120 radiations per second for the fission noise driving function. The white fission noise excited spectral density also exhibits a steeper initial slope.

These differences in the shapes of the neutron flux spectral densities are illustrated by Figure 5, which is a plot of the ratio of the two functions versus the frequency. If the two spectral densities were of the same shape, the ratio would be constant. Figure 5 shows that for frequencies greater than about 0.1 radians per second the shapes of the two functions are the same, but as the frequency decreases below 0.1, the shapes become increasingly different from one another.

Although the difference between these two functions is not great, it is interesting to recognize its existence. This difference may be due to the fact that the two driving

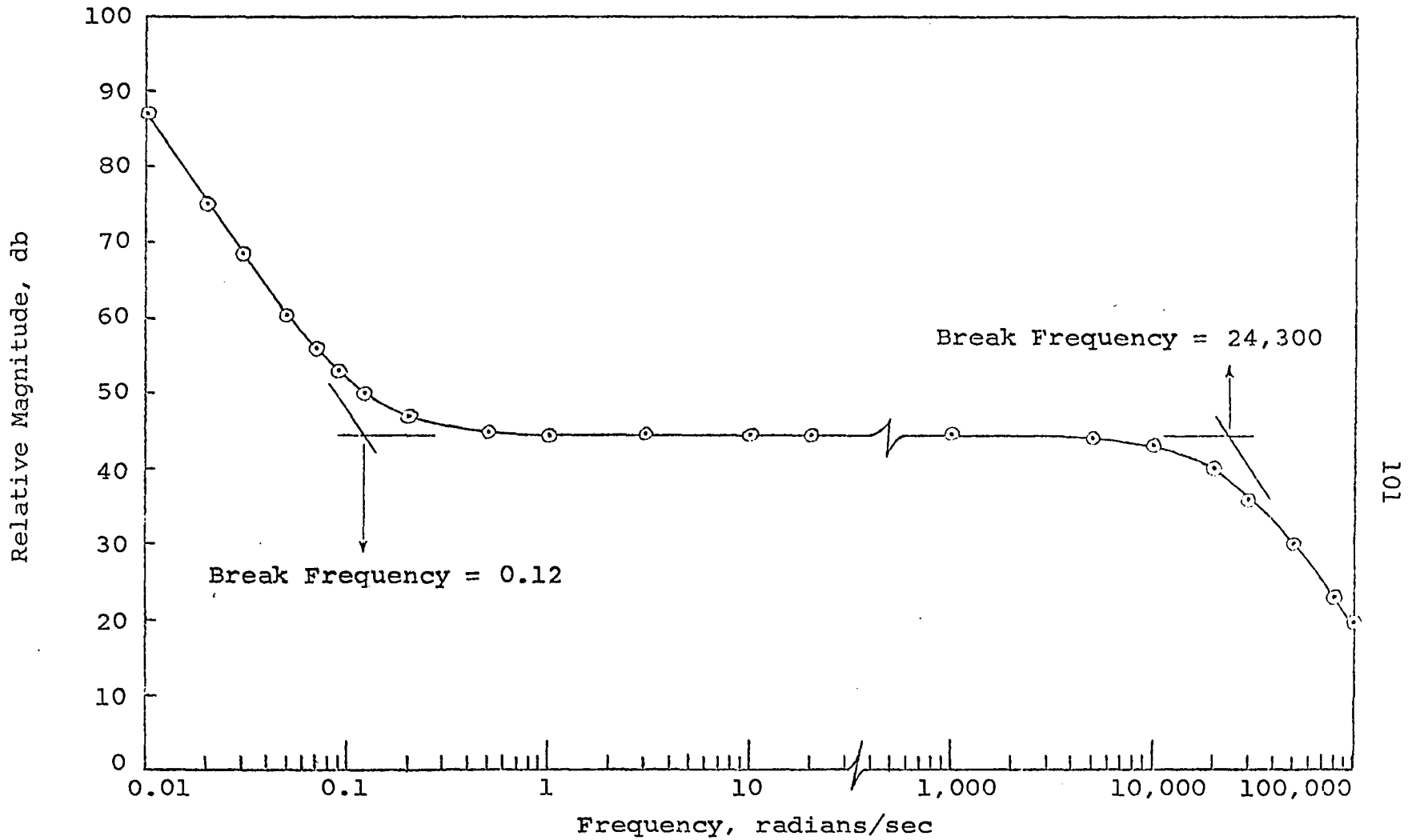

Figure 4. Neutron flux spectral density for white fission noise

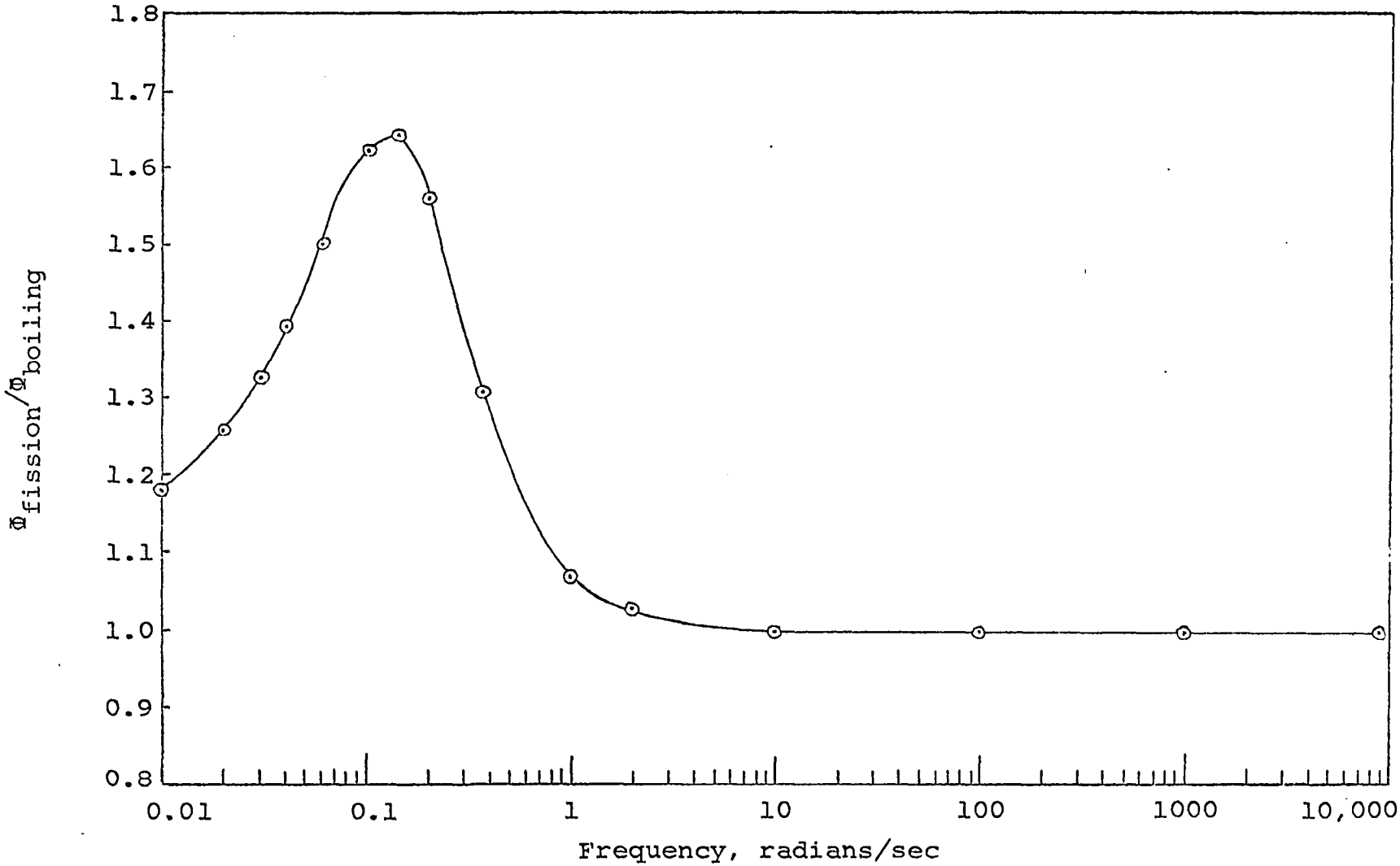

Figure 5. Ratio of $\Phi_{fission}$ to $\Phi_{boiling}$ as a function of frequency

functions affect different parameters and appear in different elements of the perturbation matrix. Consequently, boiling appears to affect the neutron flux noise in the reactor system in a slightly different manner than the inherent reactor fission-type induced noise.

Several series of test conditions were considered in an effort to determine the spatial dependence input driving functions. Each test consisted of the calculation of four spectral density functions for the given input driving function. The four spectral functions calculated correspond to 1) spectral density, i.e., both detectors placed at $\vec{r}_1$ with $E_1 = E_2$, 2) energy cross spectral density, i.e., both detectors at $\vec{r}_1$ with $E_1 \neq E_2$, 3) spatial spectral density, i.e., a detector at $\vec{r}_1$ and $\vec{r}_2$ with $E_1 = E_2$, and 4) spatial-and-energy cross spectral density, i.e., detectors at $\vec{r}_1$ and $\vec{r}_2$ with $E_1 \neq E_2$. The results of such a test are presented in Figure 6. These curves are numbered 1 through 4 corresponding to the four arrangements just described. The magnitude of the flux spectral densities are plotted in decibels, db, versus the frequency. A decibel is a measure of the magnitude defined as 20 times $\log_{10}$ of the magnitude.

It is observed that by forming the energy cross spectral density function at $\vec{r}_1$ (run no. 2), the output magnitude is increased by about 21 db over the conventional spectral density (run no. 1). Thus, for this model, energy cross

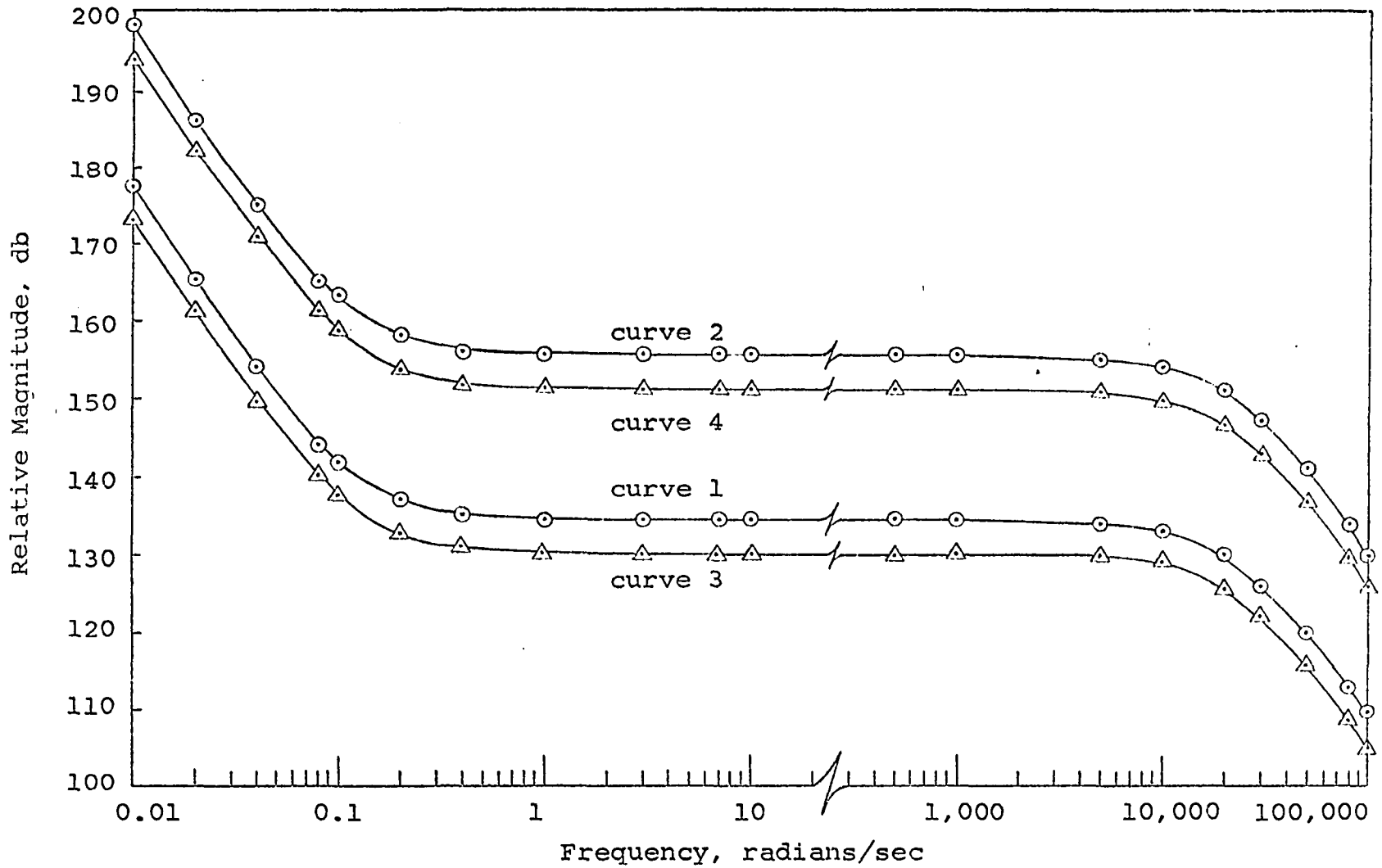

Figure 6. Neutron flux spectral density functions

correlation increases the sensitivity of the measurements.

When applied to the problem of sodium boiling detection, this increased sensitivity may allow the detectors to be placed in a location more removed from the extreme radiation and temperature fields present in the core of the reactor. This would reduce the demands on the detector system and may consequently increase its reliability.

Run 3 demonstrates that by moving one of the detectors from $\vec{r}_1$ to $\vec{r}_2$, the spectral density decreases by approximately 4.3 db. Leaving the detectors so placed, an energy cross spectral density then increases the previous magnitude by approximately 21 db.

This 21 db increase, resulting from forming an energy cross spectral density, is due to the difference in the group 1 and group 2 neutron flux magnitudes. The neutron flux of group 2 is greater than the group 1 flux by a factor of approximately 11. As the difference in the magnitude of the two energy group fluxes increases, the energy cross spectral density function increases in magnitude. Thus, the sensitivity increases as the difference between the magnitudes of the two energy group fluxes increases.

The energy spectrum of the neutron flux in a fast sodium cooled reactor possesses a peak at about 300 kev and a dip due to the sodium scattering reasonance, at approximately 3 kev. Thus, if energy cross spectral density

measurements could be made of the flux in narrow energy groups centered at about 300 and 3 kev, the sensitivity should be significantly increased. When boiling occurs, the scattering from high to low energies is reduced and this effect may give an indication of the presence of boiling.

Many series of test conditions for various driving functions were studied. The driving functions considered were: 1) uniformly distributed white fission noise, 2) localized white boiling noise, 3) localized white boiling noise which is zero above a frequency of 20 radians per second, 4) localized boiling with the spectral density shown in Figure 1 and 5) combinations of the above.

None of these test conditions exhibited any space dependence other than the magnitude effect mentioned above. The white boiling driving function yielded the same results as the white fission noise except for a difference in magnitude. The relative magnitudes between the four spectral functions calculated for a given driving function remained the same for all driving functions.

The effect of boiling on the neutron flux spectral density is demonstrated by Figure 7. Curve 1 corresponds to the occurrence of white fission noise only. When boiling with a white spectral density cutting off at 20 radians per second is simulated to occur also, curve 2 results. Thus,

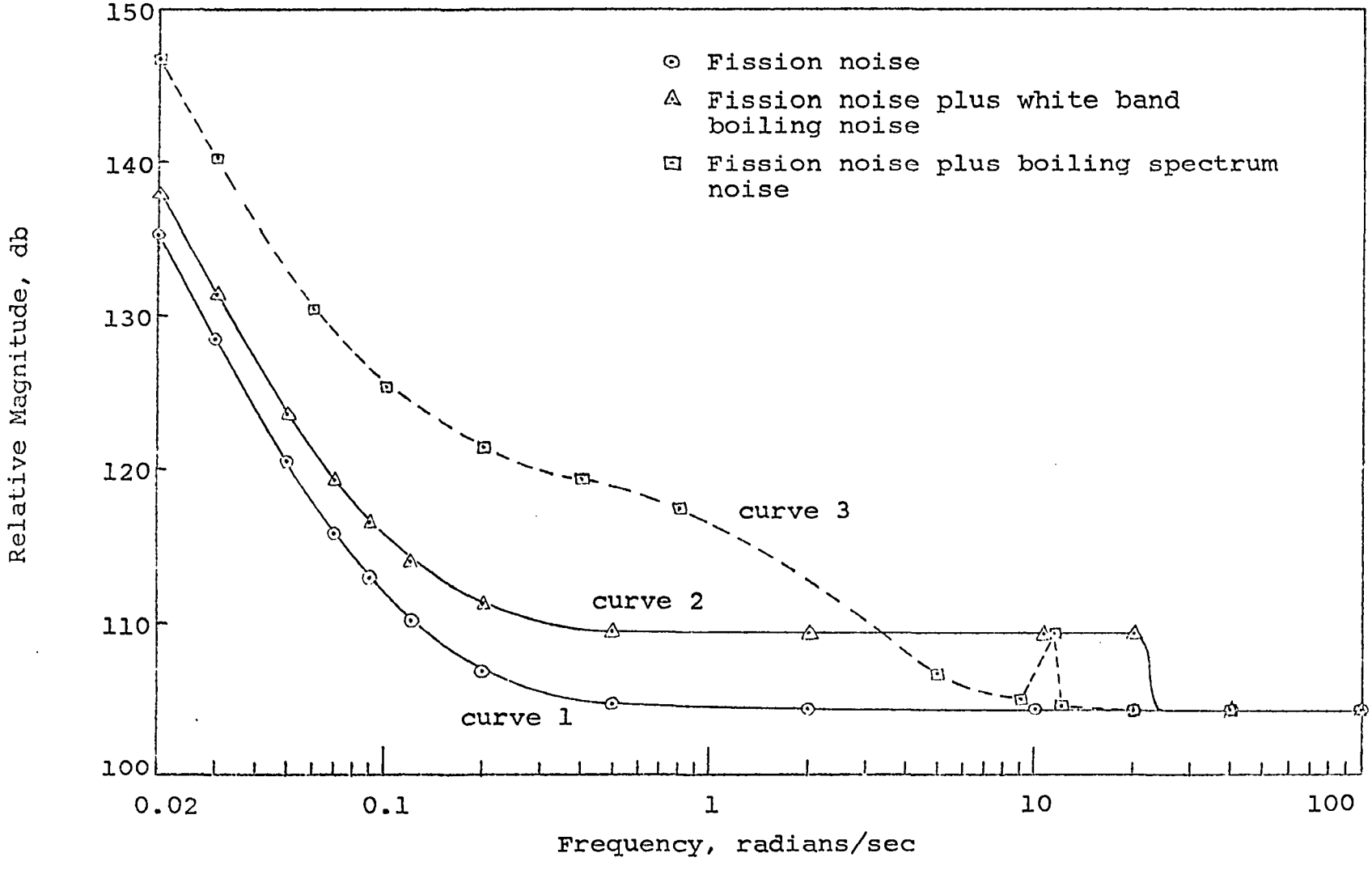

Figure 7. Neutron flux spectral density for three different driving functions

if boiling is characterized by this behavior, it would excite a general increase in the neutron flux noise level for frequencies below the cut-off. The presence of this increase along with the discrete cut-off could then be employed to detect boiling.

Curve 3, of Figure 7, results from using the boiling spectral density spectrum of Figure 1. In this case, boiling produces a distinct and characteristic change in the neutron flux spectral density. Consequently, according to this model, the appearance of the sharp peak at about 10 radians per second, and the increase in noise for lower frequencies, would indicate that the sodium was boiling in the reactor core. Of course the neutron flux noise produced by boiling must be of the same order of magnitude as that of the fission noise if the effect of boiling is to be "seen".

As the localized boiling volume increases, one would expect the magnitude of the excited neutron flux noise to increase also. This behavior is illustrated by the results in Figure 8. The lower curve is due to fission noise alone; the other curves demonstrate how the boiling induced flux noise increases with increasing volume of boiling. As more sodium boils, the effect on the neutron flux spectral density becomes more pronounced.

The results of the simple feedback model are displayed in Figure 9. Curve A represents the results with no feedback

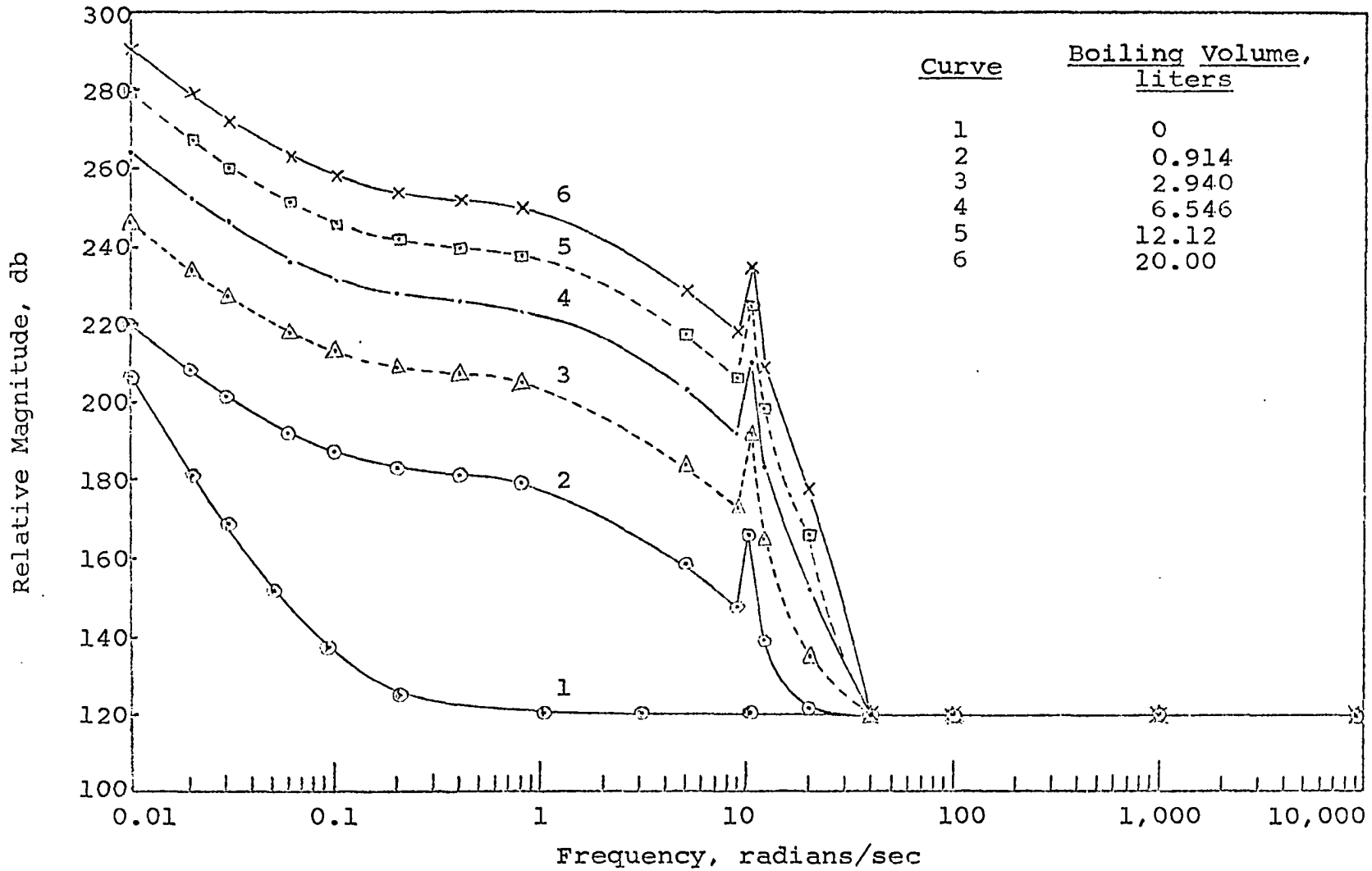

Figure 8. Effect of boiling volume on neutron flux spectral density

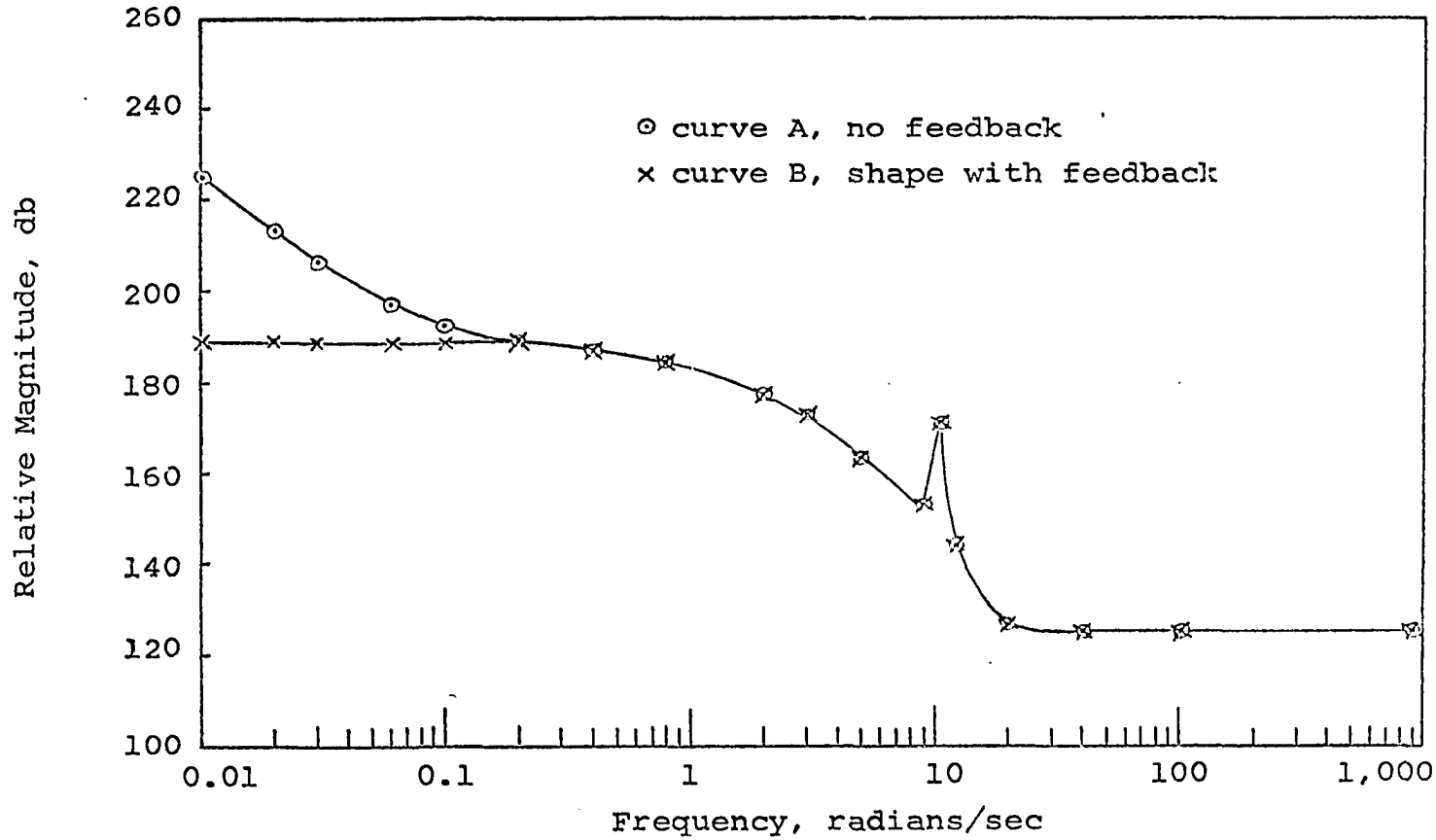

Figure 9. Effect of feedback on shape of neutron flux spectral density

and curve B illustrates how the shape of the results are altered by the feedback effect. It is important to note that the feedback is a stabilizing phenomenon and consequently, it in effect reduces the magnitude of the perturbation. This results not only in a change in the shape of the spectral density, but also in a reduction in magnitude for all frequencies. The qualitative result of the shape change is what is desired here and it is for this reason that both curves converge for frequencies above about 0.1 radian per second.

The results, based on this particular model, demonstrated in Figures 8 and 9 lead to a suggested method for detecting the occurrence of boiling in a sodium cooled fast reactor. This technique is based on monitoring the difference or ratio of the neutron flux spectral density of two different frequencies. Figure 8 shows how boiling increases the low frequency (< 12 rad/sec) segment of the spectral density while the high frequency segment (above 12 rad/sec) is essentially unaffected. Figure 9 demonstrates how feedback levels off the very low frequency end while not affecting the shape for frequencies above about 0.1 radians per second. It is also observed that the spectral density due to fission noise is flat above about 0.5 radians per second. Thus, by monitoring the difference in the flux spectral density at 0.5 radians per second, Φ_1,

and the value at 100 radians per second, Φ_2, an indication of the presence of boiling can be obtained.

Figure 10 demonstrates the behavior of the method suggested utilizing the results presented in Figure 8 for increasing boiling volume. The value of $\Phi_1 - \Phi_2$ is very sensitive to the volume of boiling for volumes up to about 1 liter, then the difference, $\Phi_1 - \Phi_2$, increases less rapidly with increasing boiling. However, for a boiling volume of 20 liters the difference is quite large, 132 db, and this corresponds to boiling in only about 0.5% of the core volume. Based on the model used in these calculations it appears that this may be a feasible means of detecting boiling in a fast sodium cooled reactor. The method requires no knowledge of the characteristics of the boiling spectral density other than that it is a low-frequency phenomenon.

In summary, the results of the model used in this investigation indicate that neutron flux noise measurements may be a feasible method for detecting boiling in a sodium cooled fast reactor. This may be done by recognizing the appearance of a characteristic spectrum due to boiling such as shown in Figure 8, or by comparing the spectral density for different frequencies as discussed. In both cases, successful detection depends on the neutron flux noise excited by boiling being of the same order of magnitude as other background neutron flux noise.

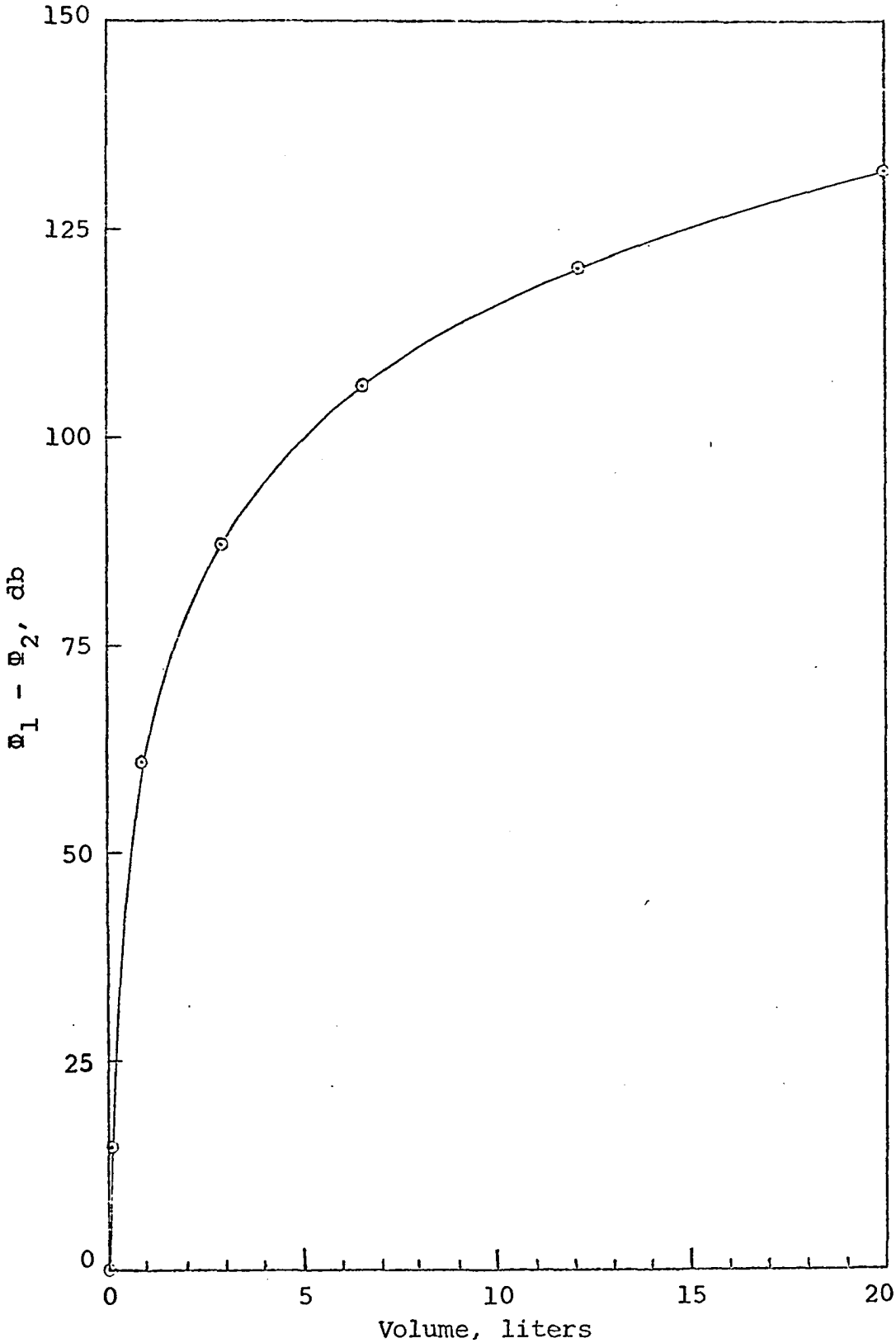

Figure 10. Effect of boiling on neutron flux noise level

It also is evident from this model that forming an energy cross spectral density increases the sensitivity and may thus permit placing the detectors outside the radiation and temperature environment of the reactor core.

Unfortunately, the results indicate that due to boiling being a low frequency phenomenon, there are no space dependent effects which could be utilized to locate the boiling, as well as detect it. However, location of the boiling might be accomplished by observing the spatial dependence of the magnitude of the neutron flux noise. That is, detectors near the boiling will indicate more of an increase in the noise level than those detectors farther away from the localized boiling. Consequently, by noting the magnitude response of a grid of detectors it may be possible to locate the general area where boiling is taking place.

The method employed for boiling detection in a fast sodium-cooled reactor will probably depend on the particular reactor system. In a fast reactor with a high background of acoustic noise (pump noise, hydraulic noise, vibrations, etc.) the neutron flux noise measurements may be the most sensitive method available. In another instance, the opposite may be true.

VII. SUGGESTIONS FOR FURTHER STUDY

It would be interesting to carry out the noise analysis using a three (or more) energy group model so that the behavior of the flux near the energy of the sodium scattering resonance could be observed in more detail. The cross spectral densities between energy groups may then yield more information.

Another extension would be to consider the effect of a reflector on the results. Since there appears to be very little space-frequency dependence, a simpler kinetics model could be used in conjunction with a more complex geometry.

More knowledge on the spectral content of sodium boiling is important if detection is to be based on recognizing a shape in the flux spectral density which is characteristic of boiling. If measurements of the spectral density of the void content in boiling sodium could be measured, the results could be used as an input to this model.

Extending the noise formulation to take into account the effect of the many positive and negative feedback mechanisms which are involved might be revealing.

VIII. ACKNOWLEDGMENTS

Many individuals are responsible for the successful completion of the graduate program culminated by this dissertation. The author wishes to express his gratitude to Dr. Glenn Murphy and Dr. Richard Danofsky, who have contributed much appreciated advice and encouragement throughout his graduate school career.

The author gratefully acknowledges support from the United States Atomic Energy Commission, who through the Oak Ridge Associated Universities, awarded an AEC Special Fellowship.

It is also appropriate to acknowledge the gratitude to Richard C. Vaughn for his confidence in the author's ability and his many encouraging discussions leading to the decision to enter graduate school.

Special thanks are due to the author's wife, Dianna, and his son, Matthew, for their many sacrifices, constant encouragement and understanding during the course of the author's college career.

IX. LITERATURE CITED

1. Ma, Benjamin M. Introductory Survey of Basic Design and Fuel-Element Considerations for Large, Fast Sodium-Cooled Reactors. Nuclear Engineering and Design 7: 399-410. 1968.

2. Creagon, Robert J. Fast Neutron Breeder Economics. United States Atomic Energy Report ANL-6792: 419-433 [Argonne National Laboratory, Argonne, Ill.] 1963.

3. Coburn, D. B. The Gas-Cooled Fast-Breeder Reactor Why and When. United States Atomic Energy Commission Report GA-8811 [Gulf General Atomic Inc., San Diego, Calif.] 1968.

4. Webb, R. A. and D. C. Schluderberg. Steam Cooling for Fast Reactors. United States Atomic Energy Commission Report ANL-7120: 136-140 [Argonne National Laboratory, Argonne, Ill.] 1965.

5. LMFBR Program Office Argonne National Laboratory. Liquid Metal Fast Breeder Reactor Program, Sodium Technology. United States Atomic Energy Commission Report WASH-1105 [Atomic Energy Commission, Washington, D.C.] August 1968.

6. Hummel, H. H., Kvitek, L., Phillips, K. E. and A. L. Rago. Sodium Void Effect. United States Atomic Energy Report ANL-7010: 86 [Argonne National Laboratory, Argonne, Ill.] 1965.

7. Kato, W. Y., Rusch, G. K. and F. H. Helm. Sodium Void Coefficients. United States Atomic Energy Report ANL-7010: 598-602 [Argonne National Laboratory, Argonne, Ill.] 1965.

8. Helm, F. and A. Travelli. Calculation of the Sodium-Void Effect in Large Carbide Cores. United States Atomic Energy Commission Report ANL-7320: 369-374 [Argonne National Laboratory, Argonne, Ill.] 1966.

9. Travelli, A. A Simple Flux-Synthesis Method for the Calculation of the Sodium-Void Effect in Reflected Single-Zone Fast Breeder Reactors. United States Atomic Energy Report ANL-7310: 205-208 [Argonne National Lab., Argonne, Ill.] 1968.

10. Etherington, Harold, ed. Nuclear Engineering Handbook. New York, New York, McGraw-Hill Book Co., Inc. 1958.

11. Okrent, D., Cohen, K. P. and W. B. Lowenstein. Some Nuclear and Safety Considerations. In the Design of Large Fast Power Reactors. Proceedings of the Third International Conference on the Peaceful Uses of Atomic Energy, Geneva, 6: 267. 1964.

12. Judd, A. M. Loss-of-Coolant Accidents in a Large Sodium-Cooled Fast Reactor. United States Atomic Energy Commission Report ANL-7120: 67-81 [Argonne National Laboratory, Argonne, Ill.] 1965.

13. Semeria, R. Sodium Boiling in the Core of Fast Reactors (Translated title). L'ebullition du sodium dans le coeur des reacteurs a neutrons rapides. Bull. Inform. Sci. Tech. (Paris), No. 122: 19-23. 1968. Original not available; translated by Argonne National Laboratory, Argonne, Ill., ANL-TRANS 625. 1968.

14. Eppler, E. P. and D. P. Roux, coordinators. Incipient Failure Diagnosis For Assuring Safety and Availability of Nuclear Power Plants, Conference Proceedings, Gatlinburg, Tennessee, October 30 - November 1, 1967. United States Atomic Energy Commission Report CONF-671011 [Division of Technical Information Extension, Atomic Energy Commission] 1967.

15. Smidt, D., Fette, P., Peppler, W., Schlechtendahl, E. G. and F. G. Schultheiss. Problems of Sodium Boiling in Fast Reactors. United States Atomic Energy Report EURFNR-564 [United States-Euratom Fast Reactor Exchange Program]. 1968.

16. Pinchera, G. C., Tomasetti, G., Falzetti, L. and G. Fornari. Sodium Boiling Researches Related to Fast Reactor Safety. American Nuclear Society Transactions 11: 691-692. 1968.

17. Logan, D., Landoni, J. and C. Baroczy. Nuclear Safety (Kinetics), Boiling Studies for Sodium. United States Atomic Energy Commission Report AI-AEC-12721 [Atomics International Division, North American Rockwell, Inc., Canoga Park, Calif.] 1968.

18. Logan, D., Randall, R. L., Baroczy, C. J. and J. A. Landoni. Boiling Liquid Metals and Two-Phase Flow Investigations. United States Atomic Energy Commission Report NAA-SR-MEMO-12485 [North American Aviation, Inc., Downey, Calif.] 1968.

19. Singer, Ralph M. The Expulsion of Liquid From A Rapidly Heated Channel. United States Atomic Energy Commission Report ANL-7337 [Argonne National Laboratory, Argonne, Ill.] 1967.

20. Singer, Ralph M. Coolant Dynamics. United States Atomic Energy Commission Report ANL-7427 [Argonne National Laboratory, Argonne, Ill.] 1968.

21. Holtz, Robert E. and Ralph M. Singer. On the Superheating of Sodium at Low Heat Fluxes. United States Atomic Energy Commission Report ANL-7383 [Argonne National Laboratory, Argonne, Ill.] 1967.

22. Lurie, H. and R. C. Noyes. Boiling Studies for Sodium Reactor Safety Part II. United States Atomic Energy Commission Report NAA-SR-9477 [North American Aviation, Inc., Canoga Park, Calif.] 1964.

23. MacFarlane, Donald R. An Analytic Study of the Transient Boiling of Sodium in Reactor Coolant Channels. United States Atomic Energy Commission Report ANL-7222 [Argonne National Laboratory, Argonne, Ill.] 1966.

24. _____ Transient Sodium Boiling Calculations - II. Nuclear Engineering and Design 6: 103-114. 1967.

25. _____ Transient Vaporization of Sodium in Reactor Coolant Channels. United States Atomic Energy Commission Report ANL-7310 [Argonne National Laboratory, Argonne, Ill.] 1968.

26. Edwards, J. A. and H. W. Hoffman. Superheat with Boiling Alkali Metals. United States Atomic Energy Commission Report ANL-7100: 515-534 [Argonne National Laboratory, Argonne, Ill.] 1965.

27. Noyes, R. C. Remarks on Some Aspects of FBR Thermal and Hydraulic Analysis: Core Optimization, Safety and Sodium Boiling. Report RT/ING(68)7 [Italy. Comitato Nazionale per l'Energie Nucleare, Rome] 1968.

28. Logan D., Landoni, J. and C. Baroczy. Nuclear Safety (Kinetics) Boiling Studies. United States Atomic Energy Commission Report AI-AEC-12680 [Atomics International, Division of North American Rockwell, Inc., Canoga Park, Calif.] 1968.

29. Atomics International, Division of North American Rockwell. Annual Technical Progress Report AEC Unclassified Programs, 1967. United States Atomic Energy Commission Report NAA-SR-12492 [North American Aviation, Inc., Canoga Park, Calif.] 1967.

30. _____ Quarterly Technical Progress Report AEC Unclassified Programs, July-September 1967. United States Atomic Energy Commission Report NAA-SR-12570 [North American Aviation, Inc., Canoga Park, Calif.] 1967.

31. Heineman, J. B. Forced Convection Boiling Sodium Studies at Low Pressure. United States Atomic Energy Commission Report ANL-7100 [Argonne National Laboratory, Argonne, Ill.] 1965.

32. Judd, A. M. Analysis of the Transient Boiling of Liquid Metals. British Journal of Applied Physics, Journal of Physics D, Series 2, No. 2, 2: 261-274. Feb. 1969.

33. Claxton, K. T. Influence of Radiation on the Inception of Boiling in Liquid Sodium. United States Atomic Energy Commission Report CONF-670916 [Division of Technical Information Extension, Atomic Energy Commission] 1967.

34. Boyd, L. R. Ion Chamber Can Detect Nucleate Boiling. Nucleonics 17, No. 3: 96-102. March 1959.

35. Collier, J. G. and P. G. Kosky. Natural Convective Boiling of the Alkali Metals - A Critical Review. Report AERE-R-5436 [Great Britain Atomic Energy Research Establishment, Harwell, Berks, England] 1967.

36. Zuber, N. Hydrodynamic Aspects of Boiling Heat Transfer. United States Atomic Energy Commission Report AECU-4439 [Division of Technical Information Extension, AEC] June 1959.

37. Rajagopal, V. Reactivity Noise Analysis as a Possible Tool for Diagnosis of Operational Malfunctions. United States Atomic Energy Commission Report CONF-671011 [Division of Technical Information Extension, Atomic Energy Commission] 1968.

38. Cook, W. H. Boiling Density Studies in Multiple Rectangular Channels. United States Atomic Energy Commission Report BNL-2446 [Brookhaven National Lab., Upton, New York] 1954.

39. Hooker, H. H. and G. F. Popper. A Gamma-Ray Attenuation Method for Void Fraction Determination in Experimental Boiling Heat Transfer Test Facilities. United States Atomic Energy Commission Report ANL-5766 [Argonne National Lab., Argonne, Ill.] 1958.

40. O'Brian, J. F. Quarterly Progress Report Number Seven. United States Atomic Energy Commission Report MND-E-2005 [Martin Co., Nuclear Division, Baltimore] January-March 1959.

41. Gouse, S. W. Methods of Measuring Void Fractions. United States Atomic Energy Commission Report NAA]SR-MEMO-5597 [North American Aviation, Inc., Canoga Park, Calif.] 1960.

42. Wentz, L. B., Neal, L. G. and R. W. Wright. X-Ray Measurement of Void Dynamics in Boiling Liquid Metals. United States Atomic Energy Commission Report ANL-7100: 195-215 [Argonne National Lab., Argonne, Ill.] 1965.

43. Balzhiser, Richard E. and Lowell R. Smith. Instrumentation For Two Phase Metallic Flows. United States Atomic Energy Commission Report ANL-7100: 217-245 [Argonne National Lab., Argonne, Ill.] 1965.

44. Ferrell, J. K. and John W. McGee. An Accurate One-Shot Gamma Attenuation Technique for Measuring Void Fractions. United States Atomic Energy Commission Report ANL-7100: 247-269 [Argonne National Lab., Argonne, Ill.] 1965.

45. Rouhani, S. Zia. Application of the Turbine Type Flow Meters in the Measurement of Steam Quality and Void. United States Atomic Energy Commission Report CONF-640607 [Division of Technical Information Extension, AEC] 1964.

46. Katz, K., Esper, Richard, T. and Walter E. Hopkins, Jr. Nucleate Boiling Detection Techniques. United States Atomic Energy Commission Report WAPD-T-588 [Westinghouse Electric Corp., Atomic Power Div., Pittsburg] 1957.

47. Jens, W. H. and P. A. Lottes. Analysis of Heat Transfer, Burnout, Pressure Drop and Density Data for High Pressure Water. United States Atomic Energy Commission Report ANL-4627 [Argonne National Lab., Argonne, Ill.] 1951.

48. Hogan, J. M. and Boyd, L. R. Joint Bettis-KAPL Nucleate Boiling Detection Experiment. United States Atomic Energy Commission Report WAPD-168 [Westinghouse Electric Corp. Atomic Power Div., Pittsburg] 1957.

49. Boyd, L. R. Nucleate Boiling Detection System Design Description. United States Atomic Energy Commission Report KAPL-M-SSD-46 [Knolls Atomic Power Lab., Schenectady, New York] 1957.

50. _____ Ion Chamber Can Detect Nucleate Boiling. Nucleonics 17, No. 3: 96-102. March 1959.

51. Spigt, C. L., Wamsteker, A. J. J. and H. F. van Valaardigen. The Application of the Impedance Method For Transient Void Fraction Measurement and Comparison With the γ-Ray Attenuation Technique. United States Atomic Energy Commission Report CONF-640607 [Division of Technical Information Extension, AEC] 1964.

52. Orbeck, I. The Impedance Void Meter. United States Atomic Energy Commission Report CONF-640607 [Division of Technical Information Extension, AEC] 1964.

53. Björkman, J. and S. Rundquist. Development of Impedance-Type Void Instruments. United States Atomic Energy Commission Report CONF-640607 [Division of Technical Information Extension, AEC] 1964.

54. Randall, R. L. Noise Analysis Instrumentation. United States Atomic Energy Commission Report AI-AEC-12680 [Atomics International, Canoga Park, Calif.] 1968.

55. Saxe, R. F. Survey of Boiling Detection Methods in Reactors. United States Atomic Energy Commission Report CONF-671011: 41-55 [Division of Technical Information Extension, AEC] 1968.

56. Evans, P. B. F. Instrumentation Problems in P.F.R. United States Atomic Energy Commission Report NP-17649, 2 [Division of Technical Information Extension, AEC] 1968.

57. Greebler, P., General Electric Co., San Jose, California. (Private Communication) 1968.

58. Barclay, F. J. and T. J. Ledwidge. Some Modern Developments in Nuclear Power. Paper presented at IEE, North Midlands Centre. February 1967.

59. Swanson, D. C., Wood, M. R. and R. R. Cone. Fast Flux Test Facility Instrumentation and Control Program. United States Atomic Energy Commission Report ANL-7380: 4-8 [Argonne National Lab., Argonne, Ill.] 1967.

60. Knox, A. E. and G. F. Popper. ANL Participation in the FFTF Instrument Development Effort. United States Atomic Energy Commission Report ANL-7380: 9-14 [Argonne National Lab., Argonne, Ill.] 1967.

61. Saxe, R. F. and L. W. Lau. An Accoustical and Optical Study of Cavitation Noise. Unpublished Ph.D. thesis. Raleigh, North Carolina, Library, North Carolina State University. 1967.

62. Rallis, C. J. and H. H. Jawurek. The Mechanisms of Nucleate boiling. Peaceful Uses of Atomic Energy, Proceedings of the Third International Conference 8: 156-163. 1964.

63. Lord Rayleigh. On the Pressure Developed in a Liquid During the Collapse of a Spherical Cavity. Philosophical Magazine [London, England] 34: 94. 1917.

64. Plesset, M. S. Dynamics of Cavitation Bubbles. Applied Mechanics 16: 277. 1949.

65. Forrester, H. K. and N. Zuber. Growth of a Vapour Bubble in a Super-heated Liquid. Journal of Applied Physics 25: 474-478. 1954.

66. Plesset M. S. and S. A. Zwick. The Growth of Vapour Bubbles in Superheated Liquids. Journal of Applied Physics 25: 493-500. 1954.

67. Minnaert, M. On Musical Air Bubbles and the Sounds of Running Water. Philosophical Magazine [London, England] 16, No. 7: 235. 1933.

68. Strasberg, M. Gas Bubbles as Sources of Sound in Liquids. Journal of the Accoustical Society of America 28, No. 1. 1956.

69. James, L. C. Experiments on Noise as an Aid to Reactor and Plant Operation. Nuclear Engineering 10: 18-22. January 1965.

70. Columb, A. L. and F. T. Binford. The Detection of Boiling in a Water-Cooled Nuclear Reactor. United States Atomic Energy Commission Report ORNL-TM-274 [Oak Ridge National Lab., Tenn.] 1962.

71. Macleod, I. D. Some Measurements of the Accoustic Spectrum Produced by Sub-Cooled Nucleate Boiling. United Kingdom Atomic Energy Authority Report TRG-Report-1205(R) [United Kingdom Atomic Energy Authority. Reactor Group. Atomic Energy Research Establishment. Harwell, Berks, England] 1966.

72. Schwartz, F. L. and L. G. Siler. Correlation of Sound Generation and Heat Transfer in Boiling. Journal of Heat Transfer 87: 436. 1965.

73. Ledwidge, Thomas Joseph. Detection of Liquid Boiling in a Nuclear Reactor. British Patent 1,052,239. Dec. 21, 1966. Abstracted in Nuclear Science Abstracts 21: 21821. 1967.

74. Clayton, J. R. Effects of Container Geometry on the Frequency of Accoustical Boiling Noise. United States Atomic Energy Commission Report IDO-17234: 21-25 [Idaho Operations Office, AEC] 1966.

75. Walton, A. J. Sonic Methods For P.F.R. Channel Blockage Detection. United Kingdom Atomic Energy Authority Report TRG-Report-665(R) [United Kingdom Atomic Energy Authority. Reactor Group. Risley, Warrington, Lancashire] 1963, reprinted 1966.

76. Anderson, T. T., Selner, R. H. and S. L. Halverson. Instrumentation and Control. In Reactor Development Program Progress Report. United States Atomic Energy Commission Report ANL-7561: 99-100 [Argonne National Lab., Argonne, Ill.] June 1969.

77. Aeroprojects Incorporated. Applications of Altrasonic Energy: Ultrasonic Instrumentation for Nuclear Applications. United States Atomic Energy Commission Report NYO-10559 [New York Operations Office, AEC] Westchester, Pa. Author. 1963.

78. Kartluke, Herbert. Ultrasonic Instrumentation for Detection of Incipient Boiling in Liquid Metals. United States Atomic Energy Commission Report NYO-3622-20 [New York Operations Office, AEC] 1968.

79. DePrisco, C. F., Kartluke, H., Maropis, N. and W. B. Tarplay. Ultrasonic Instrumentation in Nuclear Applications: I, Ultrasonic Detection of Incipient Boiling and Cavitation. United States Atomic Energy Commission Report NYO-10010 [New York Operations Office, AEC] 1962.

80. Maropis, N. Method and Apparatus for Detecting ImminentBoiling. British Patent 1,064,662. August 5, 1967. Abstracted in Nuclear Science Abstracts 21: 20014. 1967.

81. Moore, M. N. The Determination of Reactor Transfer Functions from Measurements at Steady Operation. Nuclear Science and Engineering 3: 387-394. 1958.

82. _____ The Power Noise Transfer Function of a Reactor. Nuclear Science and Engineering 6: 448-452. 1959.

83. Colm, C. E. Determination of Reactor Kinetic Parameters by Pile Noise Analysis. Nuclear Science and Engineering 5: 331-335. 1959.

84. _____ A Simplified Theory of Pile Noise. Nuclear Science and Engineering 7: 472. 1960.

85. Fry, D. N., Roux, D. P., Ricker, C. W., Stephenson, S. E., Hanover, S. H. and J. R. Trinko. Neutron Fluctuation Measurements at Oak Ridge National Laboratory. United States Atomic Energy Commission Report ORNL-P-1967 [Oak Ridge National Lab., Tenn.] 1967.

86. Yamada, S. and H. Kage. Reactor Noise Caused by Coolant-Flow Fluctuation. In a Symposium on Neutron Noise, Waves, and Pulse Propagation, Proceedings, University of Florida, Gainesville, 1966. Pp. 455-462. [Division of Technical Information, United States Atomic Energy Commission, Washington, D.C.] 1967.

87. Rajagopal, V. Reactivity Noise Analysis as a Possible Tool for Diagnosis of Operational Malfunctions. United States Atomic Energy Commission Report CONF-671011: 87 [Division of Technical Information Extension, AEC] 1968.

88. _____ Dynamic Measurements in PWR Power Plants. American Nuclear Society Transactions 10, No. 1: 217. June 1967.

89. Rajagopal, V. and Gallagher, J. M., Jr. Some Applications of Dynamic (Noise) Measurements in Pressurized-Water-Reactor Nuclear Power Plants. In a Symposium on Neutron Noise, Waves, and Pulse Propagation, Proceedings, University of Florida, Gainesville, 1966. Pp. 487-501. [Division of Technical Information, United States Atomic Energy Commission, Washington, D.C.] 1967.

90. Jordan, E. L. Detection of In-Core Void Formation by Noise Analysis. American Nuclear Society Transactions 9: 317. 1966.

91. Mulcahey, Thomas P., Reactor Engineering Division, Argonne National Laboratory, Argonne, Ill. Private communication. 1969.

92. Fry, D. N. and J. C. Robinson. Neutron Density Fluctuations as a Reactor Diagnostic Tool. United States Atomic Energy Commission Report CONF-671011 [Division of Technical Information Extension, AEC] 1968.

93. Weaver, Lynn E. Systems Analysis of Nuclear Reactor Dynamics. New York, New York, Rowman and Littlefield, Inc. c1963.

94. Kaplan, S. Space-Time Kinetics. In Radkowsky, A., ed. Naval Reactor Physics Handbook. Vol. 1. Pp. 955-957. Washington, D.C., U.S. Government Printing Office. 1964.

95. Keepin, G. R. Physics of Nuclear Kinetics. Reading Mass., Addison-Wesley Publishing Co., Inc. 1965.

96. Foulke, Larry R. and Elias P. Gyftopoulos. Application of the Natural Mode Approximation to Space-Time Reactor Problems. Nuclear Science and Engineering 30: 419-435. 1967.

97. Bentancourt, Joaquin Manuel. Analysis of Coupled Core Reactors Using the Natural Mode Approximation. Unpublished Ph.D. Thesis. Ames, Iowa, Library, Iowa State University. 1968.

98. Weinberg, Alvin and Eugene P. Wigner. The Physical Theory of Neutron Chain Reactors. 2ed. Chicago, Ill., The University of Chicago Press. 1959.

99. Danofsky, Richard A. Modal Analysis and the Natural Mode Approximation. Unpublished mimeographed lecture notes. Ames, Iowa, Department of Nuclear Engineering, Iowa State University of Science and Technology. 1968.

100. Henry, A. F. The Application of Inhour Modes to the Description of Non-separable Reactor Transients. Nuclear Science and Engineering 20: 338. 1964.

101. Kaplan, S. The Property of Finality and the Analysis of Problems in Reactor Space-Time Kinetics by Various Modal Expansions. Nuclear Science and Engineering 9: 357-361. 1961.

102. Sommerfeld, A. Partial Differential Equations in Physics. New York, New York, Academic Press, Inc. 1949.

103. Danofsky, R. A. A Space-Dependent Reactor-Noise Formulation Utilizing Modal Expansions. Nuclear Science and Engineering 36: 28-38. 1969.

104. Lee, Y. W. Statistical Theory of Communication. New York, New York, John Wiley and Sons Inc. 1960.

105. Miller, Kenneth S. Engineering Mathematics. New York, New York, Dover Publications, Inc. 1963.

106. Yiftah S., Okrent, D. and P. A. Moldaver. Fast Reactor Cross Sections. New York, New York, Pergamon Press. 1960.

107. Meneghetti, David. Introductory Fast Reactor Physics Analysis. United States Atomic Energy Commission Report ANL-6809 [Argonne National Lab., Argonne, Ill.] 1963.

108. Little, W. W., Jr. and R. W. Hardie. Methods for Collapsing Fast-Reactor Neutron Cross Sections. Nuclear Science and Engineering 29: 402-407. 1967.

109. Golden, G. H. Elementary Neutronics Considerations in LMFBR Design. United States Atomic Energy Commission Report ANL-7532 [Argonne National Laboratory, Argonne, Ill.] 1969.

110. Eggen, D. T. Notes on Fast Reactor Core Design Considerations. Unpublished paper presented at the 1968 AMU-NEEC Faculty-Student Conference, Argonne National Lab., Argonne, Ill., August 29, 1968. Mimeo. Evanston, Ill., Northwestern University, The Technological Institute. ca.1968.

111. Visner, Sidney. Liquid Metal Fast Breeder Reactor Design Study. Volumes 1 and 2. United States Atomic Energy Commission Report CEND-200 [Combustion Engineering, Inc., Nuclear Division, Windsor, Conn.] 1964.

112. Eggen, D. T. Feasibility Study of a 1000-Mwe Sodium-Cooled Fast Reactor. United States Atomic Energy Commission Report NAA-SR-11378 [North American Aviation, Inc., Canoga Park, Calif.] 1966.

113. Lamarsh, John R. Introduction to Nuclear Reactor Theory. Reading, Massachusetts, Addison-Wesley Publishing Co., Inc. c1966.

114. International Business Machines Corporation, Technical Publications Department. System/360 Scientific Subroutine Package (360A-CM-03X) Version III Programmers Manual. 4 ed. White Plains, New York, Author. c1968.

115. Wylie, C. R., Jr. Advanced Engineering Mathematics. 2 ed. New York, New York, McGraw-Hill Book Company, Inc. 1960.

X. APPENDIX A: EQUATIONS USED TO COLLAPSE MULTIGROUP CROSS SECTIONS TO FEW-GROUP VALUES

This appendix presents the methods used to collapse a 16-group set of fast reactor cross sections (106) to the 2-group set used in this investigation. The integrals were approximated by a standard numerical analysis technique. The resulting expressions being suitable for evaluation using a digital computer.

The flux averaged cross section for the g^{th} energy group, with lower energy limit E_L^g and upper limit E_U^g, is defined to be

$$\bar{\sigma}^g = \frac{\int_{E_L^g}^{E_U^g} \sigma(E)\phi(E)dE}{\int_{E_L^g}^{E_U^g} \phi(E)dE} \qquad (A.1)$$

where (E) is the energy dependent neutron flux. This equation serves as the basis for collapsing a "fine" 16-group structure of absorption cross sections to a "coarse" 2-group structure. Parameters referring to the fine structure will be distinguished from the coarse structure by a superscript index "f". A superscript index "c" denotes values referring to the coarse energy group structure.

Using the above notation, the fission cross section for group c can be expressed as

$$\sigma_f^{\,c} = \frac{\int_{E_L^{\,c}}^{E_U^{\,c}} \sigma_f(E)\phi(E)\,dE}{\int_{E_L^{\,c}}^{E_U^{\,c}} \phi(E)\,dE}, \qquad \text{(A.2)}$$

where $E_L^{\,c}$ and $E_U^{\,c}$ are the energy limits of group c. The integral from $E_L^{\,c}$ to $E_U^{\,c}$ can be written as a sum of integrals, each of which is over one of the fine energy groups, f, contained in group c; resulting in

$$\sigma_f^{\,c} = \frac{\sum_{\text{all f in c}} \int_{E_L^{\,f}}^{E_U^{\,f}} \sigma_f^{\,f}\phi(E)\,dE}{\sum_{\text{all f in c}} \int_{E_L^{\,f}}^{E_U^{\,f}} \phi(E)\,dE}. \qquad \text{(A.3)}$$

Note that for each of the fine energy groups, f, the energy dependent fission cross section has been replaced by the corresponding average value from the 16-group set, $\sigma_f^{\,f}$.

By replacing $\phi(E)$ with the average flux, Φ^f, for each fine energy group, the above equation becomes

$$\sigma_f^c = \frac{\sum_{\text{all f in c}} \sigma_f^f \Phi^f \Delta E^f}{\sum_{\text{all f in c}} \Phi^f \Delta E^f} , \qquad (A.4)$$

where

$$\Delta E^f = \int_{E_L^f}^{E_U^f} de$$

$$= E_U^f - E_L^f . \qquad (A.5)$$

Equation A.4 allows the employment of a digital computer to calculate the 2-group capture and fission cross sections.

The equations for determining the 2-group elastic and inelastic scattering cross sections are somewhat more complicated. The energy level diagram in Figure 11 will serve as an explanatory aid.

The average cross section for scattering (elastic or inelastic) from energy group f to some lower energy group f' can be written as

$$\bar{\sigma}^{f\to f'} = \frac{\int_{E_L^{f'}}^{E_U^{f'}} \int_{E_L^f}^{E_U^f} \sigma(E\to E')\phi(E)\,dE\,dE'}{\int_{E_L^{f'}}^{E_U^{f'}} \int_{E_L^f}^{E_U^f} \phi(E)\,dE\,dE'} . \qquad (A.6)$$

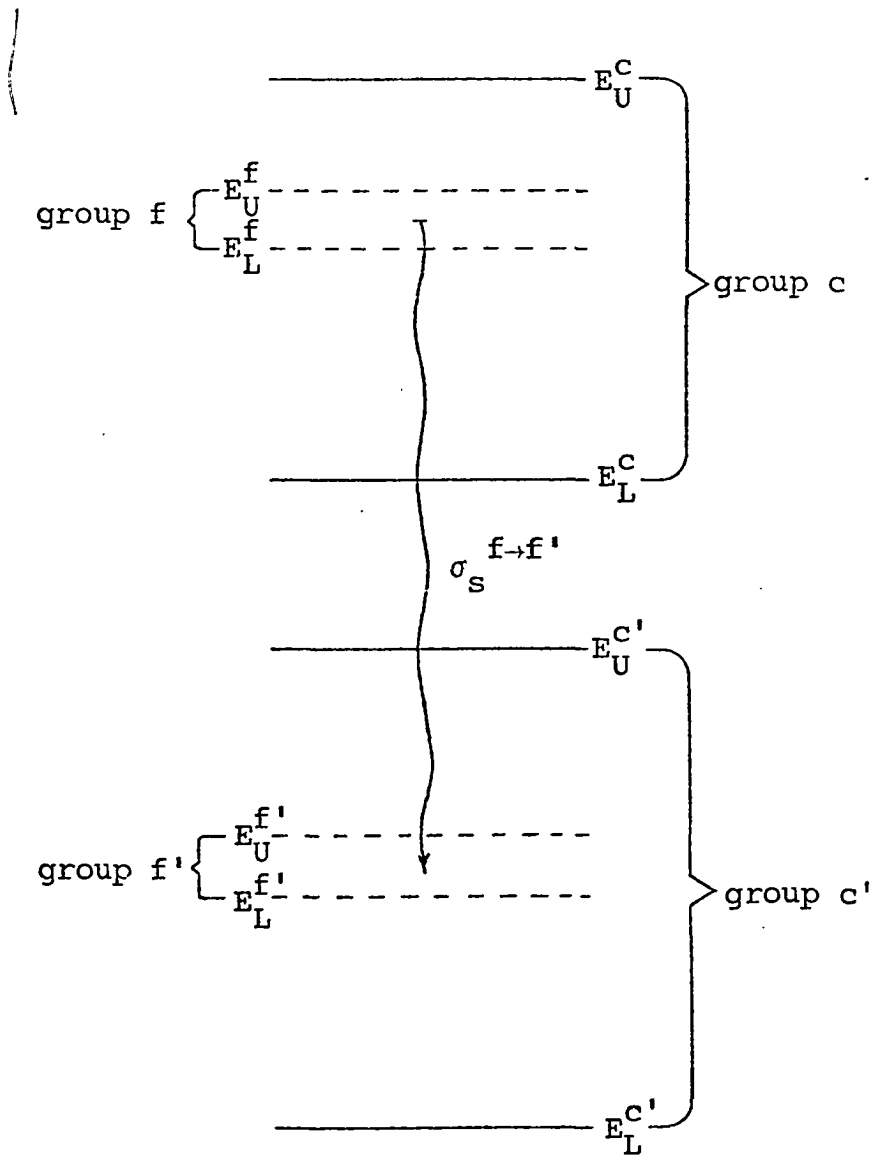

Figure 11. Energy level diagram

The cross section for scattering from any energy in group c down to any energy in group c' is denoted by $\sigma^{c\to c'}$. It is equal to the sum of all $\bar{\sigma}^{f\to f'}$, for all f in c, plus the sum of all $\bar{\sigma}^{f\to f'}$, for all f' in c'. Thus,

$$\sigma^{c\to c'} = \frac{\sum_{\text{all } f' \text{ in } c'} \sum_{\text{all } f \text{ in } c} \int_{E_L^{f'}}^{E_U^{f'}} \int_{E_L^{f}}^{E_U^{f}} \sigma(E\to E')\phi(E)\,dE\,dE'}{\sum_{\text{all } f' \text{ in } c'} \sum_{\text{all } f \text{ in } c} \int_{E_L^{f'}}^{E_U^{f'}} \int_{E_L^{f}}^{E_U^{f}} \phi(E)\,dE\,dE'} . \tag{A.7}$$

If, for the integral over E, $\sigma(E\to E)$ is replaced by the 16-group constant $\sigma^{f\to f'}$, and an average flux, Φ^f, for energy group f is substituted for $\phi(E)$, Equation A.7 becomes

$$\sigma^{c\to c'} = \frac{\sum_{\text{all } f' \text{ in } c'} \sum_{\text{all } f \text{ in } c} \int_{E_L^{f'}}^{E_U^{f'}} \sigma^{f\to f'}\Phi^f\Delta E^f\,dE'}{\sum_{\text{all } f' \text{ in } c'} \sum_{\text{all } f \text{ in } c} \int_{E_L^{f'}}^{E_U^{f'}} \Phi^f\Delta E^f\,dE'} , \tag{A.8}$$

where $E^f = E_U^f - E_L^f$. The integral over E' may now be evaluated, yielding

$$\sigma^{c\to c'} = \frac{\sum_{\text{all } f' \text{ in } c'} \sum_{\text{all } f \text{ in } c} \sigma^{f\to f'} \Phi^f \Delta E^f \Delta E^{f'}}{\sum_{\text{all } f' \text{ in } c'} \sum_{\text{all } f \text{ in } c} \Phi^f \Delta E^f \Delta E^{f'}}$$

$$= \frac{\sum_{\text{all } f' \text{ in } c'} \sum_{\text{all } f \text{ in } c} \sigma^{f\to f'} \Phi^f \Delta E^f \Delta E^{f'}}{\Delta E^{c'} \sum_{\text{all } f \text{ in } c} \Phi^f \Delta E^f} \quad ,$$

where $E^{c'} = E_U{}^{c'} - E_L{}^{c'}$. Equation A.9 is now in a form compatible with calculation on a digital computer.

The group diffusion constant is defined as

$$D(E) = 1/3\Sigma_{tr}(E)$$

where $\Sigma_{tr}(E)$ is the macroscopic transport cross section. In calculating D, it is common practice to use the flux averaged reciprocal microscopic transport cross section (107)

$$\sigma_{tr}{}^f \equiv \frac{1}{\left(\frac{1}{\sigma_{tr}}\right)^f}$$

in calculating Σ_{tr}. The same equation as used for the coarse group absorption and fission cross sections then apply, except now the reciprocals of the fine group transport cross sections are used in the calculations.

XI. APPENDIX B: EVALUATION OF PERTURBATION INNER PRODUCT

This appendix evaluates the numerator of the perturbation inner product, $n_i(t)$. It is also demonstrated that n_i may be expressed as the sum of products of mode dependent factors and time dependent factors, i.e.,

$$n_i(t) = \varepsilon_i P(t) + \eta_i W(t) \quad . \tag{B.1}$$

From Equation 106 $n_i(t)$ is expressed as

$$\begin{aligned} n_i(t) = \int_{\text{reactor}} [&\delta F_{11} V_1 \psi_i^{+1} \phi_o^1 + \delta F_{12} V_1 \psi_i^{+1} \phi_o^2 + \delta F_{21} V_2 \psi_i^{+2} \phi_o^1 \\ &+ \delta F_{22} V_2 \psi_i^{+2} \phi_o^2 + \delta F_{31} \psi_i^{+3} \phi_o^1 + \delta F_{32} \psi_i^{+3} \phi_o^2 \\ &+ \delta B_{11} V_1 \psi_i^{+1} \phi_o^1 + \psi_i^{+2} V_2 (\delta B_{21} \phi_o^1 + \delta B_{22} \phi_o^2)] dx dy dz \quad . \end{aligned} \tag{B.2}$$

where

$$\phi_o^j = F_j \sin \frac{\pi x}{a} \sin \frac{\pi y}{b} \sin \frac{\pi z}{c}$$

$$\psi_i^{+j} = e_i^{+j} \sin \frac{\ell \pi x}{a} \sin \frac{m \pi y}{b} \sin \frac{n \pi z}{c} \quad .$$

Denoting the time dependence of the fission noise perturbation by W(t) and its magnitude by N, one can write

$$\delta F = N W(t) \quad . \tag{B.3}$$

The first integral in Equation B.2 may now be evaluated;

denoting this integration by I_1, one has

$$I_1 = \int_{z=0}^{c} \int_{y=0}^{b} \int_{x=0}^{a} N W(t) V_1 e_i^{+1} \sin \frac{\ell\pi x}{a} \sin \frac{m\pi y}{b} \sin \frac{n\pi z}{c} \; x$$

$$F_1 \sin \frac{\pi x}{a} \sin \frac{\pi y}{b} \sin \frac{\pi z}{c} \, dxdydz \quad .$$

$$= N W(t) V_1 e_i^{+1} F_1 \{ \int_0^a \sin \frac{\ell\pi x}{a} \sin \frac{\pi x}{a} \, dx \} \; x$$

$$\{ \int_0^b \sin \frac{m\pi y}{b} \sin \frac{\pi y}{b} dy \} \{ \int_0^c \sin \frac{n\pi z}{c} \sin \frac{\pi z}{c} dz \} \; . \tag{B.4}$$

Consider first the integral over x, denoting this by X_{11}

$$X_{11} = \int_0^a \sin \frac{\ell\pi x}{a} \sin \frac{\pi x}{a} \, dx \quad . \tag{B.5}$$

For $\ell \neq 1$,

$$X_{11} = \frac{\sin(\ell\pi - \pi)}{2(\frac{\ell\pi}{a} - \frac{\pi}{a})}$$

$$= 0 \quad , \tag{B.6}$$

since ℓ is an integer. If $\ell = 1$, the integration is

$$X_{11} = \int_0^a \sin^2 \frac{\pi x}{a}\, dx$$

$$= \frac{a}{2} \quad . \tag{B.7}$$

Thus X_{11} is zero unless $\ell = 1$. It is seen from Equation B.4 that the second and third integrals are of the same form as X_{11}. As a result

$$Y_{11} = \begin{cases} 0 & m = 2,3,4,\ldots \\ \\ \frac{b}{2} & m = 1 \end{cases} \tag{B.8}$$

$$Z_{11} = \begin{cases} 0 & n = 2,3,4,\ldots \\ \\ \frac{c}{2} & n = 1 \end{cases} \tag{B.9}$$

With these results, one can conclude the following about I_1

$$I_1 = \begin{cases} N\, V_1 e_i^{+1} F_1 \left(\frac{abc}{8}\right) W(t), & \ell = m = n = 1 \\ \\ 0 \qquad \text{otherwise.} \end{cases} \tag{B.10}$$

The first six integrals of Equation B.2 all have the same form as I_1, thus, in general, the first six integrals are zero unless $\ell = m = n = 1$. Recall that for each mode, specified by ℓ, m and n, there are three eigenvalues

corresponds to running index values of i = 1,2,3. For i > 3, the first six integrals are zero. For i = 1,2,3, these integrals can be expressed as

$$I_1 + I_2 + \ldots + I_6 = [V_1 e_i^{+1} F_1 + V_1 e_i^{+1} F_2 + \ldots + e_i^{+2} F_2] \; x$$

$$[\frac{abc}{8} N] W(t)$$

$$= \eta_i W(t) \quad . \tag{B.11}$$

Hence, the result is the product of a mode dependent factor, η_i, and the time dependence of the perturbation, W(t).

The last three integrals in Equation B.2 correspond to localized boiling. As a result, the integration is not over the entire reactor because the perturbation is zero everywhere except over the boiling volume.

Using the expression given in Equation 104, the seventh integration of Equation B.2 will yield

$$I_7 = \int_{\substack{\text{reactor} \\ \text{perturbation}}} \{M_{11} P(t) [1-e^{-\gamma(Z-Z_L)}] V_1 e_i^{+1} \sin \frac{\ell\pi x}{a} \sin \frac{m\pi y}{b} \sin \frac{n\pi z}{c} \; x$$

$$F_1 \sin \frac{\pi x}{a} \sin \frac{\pi y}{b} \sin \frac{\pi z}{c}\} dx dy dz \quad .$$

$$= \{M_{11} P(t) V_1 e_i^{+1} F_1\} \{\int_{x_L}^{x_U} \sin \frac{\ell\pi x}{a} \sin \frac{\pi x}{a} dx\} \{\int_{u_L}^{y_U} \sin \frac{m\pi y}{b} \sin \frac{\pi y}{b} dy\}$$

$$x \left\{ \int_{z_L}^{z_U} [1-e^{-\gamma(Z-Z_L)}] \sin \frac{n\pi z}{c} \sin \frac{\pi z}{c} \, dz \right\} \qquad (B.12)$$

These integrals may be evaluated, yielding constants (for fixed x, y, and z) X_7, Y_7 and Z_7; thus

$$I_7 = M_{11} V_1 e_i^{+1} F_1 X_7 Y_7 Z_7 P(t) \quad . \qquad (B.13)$$

The last two integrals in Equation B.2 are of identical form so that

$$I_7 + I_8 + I_9 = [M_{11} V_1 e_i^{+1} F_1 X_7 Y_7 Z_7 + \ldots] P(t)$$

$$= \varepsilon_i P(t) \quad . \qquad (B.14)$$

The above results then allow one to write Equation B.2 as

$$n_i(t) = I_1 + I_2 + \ldots + I_q$$

$$= \eta_i W(t) + \varepsilon_i P(t) \quad , \qquad (B.15)$$

where

$$\eta_i \begin{cases} = 0 & i > 3 \\ \neq 0 & i = 1,2,3 \quad . \end{cases}$$